REPORT DOCUMENTATION PAGE

Form Approved
OMB NO. 0704-0188

1. AGENCY USE ONLY (Leave Blank)	2. REPORT DATE August 25, 2004	3. REPORT TYPE AND DATES COVERED Final Progress Report, June 1, 2001 -May 31 2004

4. TITLE AND SUBTITLE
A New Generation of Magneto-Rheological Fluid Dampers

5. FUNDING NUMBERS
DAAD19-01-1-0614

6. AUTHOR(S)
F. Gordaninejad, A. Fuchs, U. Dogrour, S. Karakas, Y. Liu, B. Hu, and C. Evrensel

7. PERFORMING ORGANIZATION NAME(S) AND ADDRESS(ES)
Department of Mechanical Engineering
University of Nevada, Reno
Reno, Nevada 89557

8. PERFORMING ORGANIZATION REPORT NUMBER

9. SPONSORING / MONITORING AGENCY NAME(S) AND ADDRESS(ES)

U. S. Army Research Office
P.O. Box 12211
Research Triangle Park, NC 27709-2211

10. SPONSORING / MONITORING AGENCY REPORT NUMBER

41481-EG
.2

11. SUPPLEMENTARY NOTES
The views, opinions and/or findings contained in this report are those of the author(s) and should not be construed as an official Department of the Army position, policy or decision, unless so designated by other documentation.

12 a. DISTRIBUTION / AVAILABILITY STATEMENT

Approved for public release; distribution unlimited.

12 b. DISTRIBUTION CODE

13. ABSTRACT (Maximum 200 words)

The overall goal of this three-year project was to study the performance of novel, fail-safe, magneto-rheological fluid (MRF) dampers by using innovative magneto-rheological (MR) materials for off-highway, high-payload vehicles such as the U. S. Army's HMMWV. In the past three years, significant advances were achieved in the areas of: 1) MR materials development, 2) theoretical modeling and experimental study of a new compact fail-safe MR damper, including its design and development of a full-scale prototype, 3) a full-scale experimental set up for quarter-HMMWV-model, and 4) control system development for the nonlinear MR damper system.

A systematic approach was followed to unify all efforts for this integrated research. Several new MR materials was developed and characterized that could be utilized in two new MR dampers with the same overall geometric dimensions as a regular HMMWV damper. A unique full-scale experimental set up was developed and tested. Extensive investigation was conducted on an accurate control system taking to account variation of the MR fluid's base viscosity and temperature.

14. SUBJECT TERMS

15. NUMBER OF PAGES
53

16. PRICE CODE

17. SECURITY CLASSIFICATION OR REPORT	18. SECURITY CLASSIFICATION ON THIS PAGE	19. SECURITY CLASSIFICATION OF ABSTRACT	20. LIMITATION OF ABSTRACT
UNCLASSIFIED	**UNCLASSIFIED**	**UNCLASSIFIED**	**UL**

(Continuation Sheet)

Table of Contents

Table of Contents 2

1. Statement of Problems Studied 3

2. Summary of the Most Important Results 4

2.1. Development and Characterization of New MR Materials 4
Introduction 4
Experimental Study 6
Results and discussion 9

2.2. MR Damper Analysis, Design, Fabrication and Experimental Study 12
Introduction 12
MR Damper Analysis Design 15
Results and Discussions 23

2.3. Full-Scale Study of Quarter-HMMWV-Model 26
Introduction 26
Theoretical Modeling 26
Control Algorithms 28
Experimental Results 30

3. List of Publications 34

4. Scientific Personnel 37

5. Report of Invention 37

6. References 37

7. Figures and Tables 41

1. Statement of Problems Studied

The overall goal of this three-year project was to study the performance of novel, fail-safe, magneto-rheological fluid (MRF) dampers by using innovative magneto-rheological (MR) materials for off-highway, high-payload vehicles such as the U. S. Army's HMMWV. In the past three years, significant advances were achieved in the areas of: 1) MR materials development, 2) theoretical modeling and experimental study of a new compact fail-safe MR damper, including its design and development of a full-scale prototype, 3) a full-scale experimental set up for quarter-HMMWV-model, and 4) control system development for the nonlinear MR damper system.

A systematic approach was followed to unify all efforts for this integrated research. Several new MR materials was developed and characterized that could be utilized in two new MR dampers with the same overall geometric dimensions as a regular HMMWV damper. A unique full-scale experimental set up was developed and tested. Extensive investigation was conducted on an accurate control system taking to account variation of the MR fluid's base viscosity and temperature.

2. Summary of Most Important Results

2.1 Development and Characterization of New MR Materials

Introduction

Magnetorheological fluids (MRFs) are suspensions of ferrous particles such as carbonyl iron particles, which are micron sized, and dispersed in a carrier medium [1]. The carrier fluids can be silicone oil, hydrocarbon oil or water depending on the specific application. In the absence of an applied magnetic field, MRFs exhibit Newtonian behavior. They exhibit rapid, nearly completely reversible rheological property changes when an external magnetic field is applied (this is known as the on-state). In the on-state ferrous particles are magnetically induced and aggregate to form chain-like or column-like structures parallel to the applied field. These structures restrict the flow of the fluid thereby altering the rheological properties of the suspension. The stress needed to yield these chain-like structures increases with applied magnetic field resulting in a field dependent yield stress [2]. The rheological behavior of MRF is often described by the Bingham plastic model [3].

To prevent the particles from settling or aggregating and allowing those to re-disperse more easily in the carrier fluid different additives are used to modify the surface of the carbonyl iron particles or to modify the viscosity of the carrier fluid. Carbonyl iron particles are usually coated with surfactant to reduce settling in MR fluids [4]. Organic polymers are also been used to coat the surface of iron particles [5].

In this research novel magneto-rheological-polymer gels (MRPGs) are investigated. MRPGs are a new generation of materials used in vibration control and damping devices. Wilson [6] studied MRPGs prepared by suspending iron particles in silicone gel or polyurethane gel. Adjusting the ratio of resin to cross linker and percentage of diluent can control the off-state rheology of the system. Xin also investigated static shear yield stress, off-state viscosity and sedimentation properties of similar systems [7]. In this study, MRPGs with improved redispersion performance and high temperature resistance property are investigated. This MRPG is a composite fluid of magnetic particles suspended in a polyimide gel. Polyimides are thermo-oxidatively stable materials with good chemical resistance. Polyimide gels contain cross-linked co-polyimide (CCPI) swollen in excess solvent. It's hard to stop the settling of iron particles completely since the large difference between the density of iron particles and carrier medium. However, these fluids can be used effectively in different devices, if they re-disperse quickly and completely. Rabinow pointed out that complete suspension stability was not necessary for most MR fluid devices since some devices such as MR dampers are very efficient mixing devices [8]. Therefore, re-dispersion of iron particles is very important issue in the investigation of MRPGs**.** Stabilization and re-dispersion of the carbonyl iron particles in the carrier medium are attributed to the adsorption of CCPI on the surface of the iron particles, thus sterically preventing the particles from aggregating. One of the features of MRPG is its controllable off-state viscosity. This is achieved through appropriate selection of carrier fluid and weight ratio of CCPI to solvent. CCPI gels are synthesized from dianhydride, diamine, diaminobenzonic acid and 1-4 butanediol (cross-linker in the solvent N-octyl-pyrrolidone).

Another MRPG system, which is supramolecular polymer gel, is also studied. The erm: "supramolecule" refers to a collection of atoms held together by covalent and non-covalent bonds. Supramolecule polymer is composed by non-covalent bonding including hydrogen, hydrophobic/hydrophilic, van der waals, metal coordination bond and other non-covalent bond. Of these, metal-ligand bonds exhibit both strong and directional interactions where the selection ion and ligand dictate association strength. The reversible nature of non-covalent bonds is important in this research. It may improve the durability of MRPG because even though the non-conalent bond is destructed by heat or shear stress it still can be reconstructed by self-assembling after remove the heat and shear stress. The matrix for suparmaolecular MPPG is based on zinc 2,2'; 6', 2"-terpyridine based polymer.

Experimental Study

Materials Development:

1) Iron particles

Carbonyl iron particles were produced by ISP Technologies Inc (Grade-R-2430), which comprise 99.5% pure iron and are formed by thermal decomposition of iron pentacarbonyl $Fe(CO)_5$. The size of these particles is about 5-7um.

2) Carrier fluids

The solvent is typically chosen based on its viscosity, freezing and boiling points and vapor pressure. The solvent used is N-octyl-pyrrolidone (Aldrich Chemical Company, Inc.) which has

a boiling point of 306°C, viscosity of 9cp at 20°C and a vapor pressure of less than 1.3Pa at 20°C.

3) Polymer systems

a) Synthesis of Crosslinked Co-Polyimide:

The solvent N-octyl-pyrrolidone (OP) is introduced into a moisture free reactor. 3,5-diaminobenzonic acid (DABA) (Aldrich Chemical Company, Inc.) is dissolved in the N-octyl-pyrrolidone. The 4,4'-(4,4'-isopropylidene diphenoxy)bis(phthalic anhydride) (ISBPA) (Aldrich Chemical Company, Inc.) is then added. This compound reacts for one hour at room temperature to form an anhydride terminated pre-polymer. Reactive comonomer 4,4'-methylenedianiline (MDA) (Aldrich Chemical Company, Inc.) is then added and mixed for 7 hours at room temperature to form high molecular weight polyamic acids. Imidization is performed by dehydration of the polyamic acid adding excessive acetic anhydride and N,N-dimethylaniline (Aldrich Chemical Company, Inc.) to the reaction mixture and stirred for 2-3 hours at 50°C. The temperature is then increased to 110°C for 30 minutes. This results in formation of linear co-polyimide. To synthesize cross-linked polyimide gel, the cross-linker 1-4 butanediol (Aldrich Chemical Company, Inc.) is added to the reaction mixture and kept at 170°C for 7 hours. The crosslink ratio can be controlled by the stoichiometric ratio of diaminobenzonic acid to the 4,4'-methylenedianiline used in the polymerization reaction. Synthesis of crosslinked polyimide is shown in Figure 1.

b) Synthesis of supramolecule

To a suspension of KOH in DMSO, the poly(ethylene oxide) was added. After stirring for 1 hour at 60C, a'-chloro-2,2';6',2"-terpyridine was added. The mixture was stirred for 48 hours at

60C, then, after cooling the suspension was poured into cool water. A certain amount of white precipitate was collected. Then, dissolving the precipitate into methanol, a solution of zinc acetate in methanol was added drop wise at 60C. The color changed immediately to yellow. With increasing metal ions, the viscosity of the solution raised slowly. The solution was put into carrier fluid and the temperature was kept at 60C evaporating the methanol. The carrier medium was formed. Synthesis of crosslinked supramolecule is given in Figure 2.

4) Synthesis of Crosslinked Polyimide and Supramolecular MRPG

a) Crosslinked polyimide MRPG

81 weight % carbonyl iron particles are added to the synthesized crosslinked polyimide gel and mixed at low shear rate (400 rpm) using a Servodyne Mixer (model 50003-30, Cole Parmer Instrument Company) for 30 minutes. Additives are mixed together and stirred thoroughly at 1200 rpm for 24 hours at room temperature.

b) Supramolecular MRPG

81 weight% carbonyl iron particles are added to the synthesized supramolecular gel and mixed at low shear rate (400 rpm) using a Servodyne Mixer (model 50003-30, Cole Parmer Instrument Company) for 30 minutes. Additives are mixed together and stirred thoroughly at 1200 rpm for 24 hours at room temperature.

Instrumentation

1) DSC

The DSC (Differential Scanning Calorimeter, Perkin Elmer, Pyris is used to investigate the polymerization between monomers from room temperature to 300°C at a heat rate of 10°C/min. DSC is also used to investigate the glass transition temperature which dictate the heat resistance of polymer.

2) Shear Rheometer

The off-state viscosity of MRPF was measured using Brookfield Rheometer (Model DV-111, Brookfield Engineering Laboratories Inc). The shear rate of the measurement is from zero to 85 1/sec.

3) DMA

A magneto-rheological rheometer (MCR300, Paar Physica Corporation) is used to investigate fluid rheology [9]. The measurement system includes three parts: the mechanical drive system, the electronics for data processing and a corresponding software package. Unlike a conventional rheometer, the magnetic field applied to the MRPG is generated by a built-in copper coil. The magnetic field is perpendicular to the gap filled with MRPG. The magnetic field (B) in the gap depends on the current in the coil and the material in the gap through which the flux flows. Two parallel disks with 20mm diameter and a 1mm gap are used for this study. Approximately 0.314 ml of sample is placed in the gap between the two plates. The plate-plate system, magnetic coil and rotor shaft are shown in Figure 3.

Results and Discussion

1) Yield stress testing

A change in rheological behavior results from the polarization induced in the suspended particles by application of an external magnetic field. These induced dipoles which cause the particles to align "head to tail" in chains and form columnar structures, parallel to the applied field [10]. These chain-like structures hinder the flow of the fluid thereby increasing the apparent viscosity of the suspension. The pressure needed to yield these chain-like structures increases with applied magnetic field resulting in a field-dependent yield stress. Thus the behavior of this type of controllable fluid in the post-yield region is often represented as a Bingham plastic having variable yield strength, as follows:

$$\tau = \tau_y + \eta \dot{\gamma}, \quad \tau \geq \tau_y \tag{1}$$

Where τ is the total shear stress, τ_y is field-controllable shear yield stress, η is the viscosity of the MRPG, and $\dot{\gamma}$ is the shear strain rate. In the pre-yield region, MRPG behaves as a viscoelastic solid, and therefore, the shear below the yield stress (at strains on the order of 10^{-3}) is given by:

$$\tau = G\gamma \tag{2}$$

Where G is the complex material modulus and γ is the shear strain. It has been observed that the complex modulus is also field dependent [11].

The effect of applied magnetic field on shear yield stress of the MRPG is investigated using the MR rheometer described earlier. The results of the shear stress versus strain rate under different applied magnetic flux densities for the MRPG are shown in Figure 4 and 5.

In Figure 6, dynamic yield stresses of two MRPGs and one commercially available MRF are shown as functions of the applied magnetic flux density B. The yield stress increases

significantly with an increase of magnetic flux density and it is observed to increase with a $B^{3/2}$ dependence, which is shown by the slope of 1.5 for the curve in Figure 9. The numerical and analytical model was developed by Ginder *et al*.[11-13], as follows:

$$\tau_y \propto \phi \mu_0 M_s^{\frac{1}{2}} B_0^{\frac{3}{2}} \tag{3}$$

Where $\mu_0 = 4\pi \times 10^{-7}$ Tesla-meter/ampere is the permeability in free space, ϕ is the volume fraction of carbonyl iron particles, M_s is the local saturation of magnetization and B_0 is the magnetic induction related with the external field H_0 by the following equation:

$$B_0 = \mu_0 (H_0 + M_s) \tag{4}$$

Therefore, the yield stress measured increases with a $B_0^{3/2}$ dependence and agrees with the model provided by Ginder *et al*. This sub quadratic dependence of flux density is a consequence of local saturation of magnetization in the contact region of each particle.

In Figure 6, the CCPI:OP=1:20 system shows a slightly higher yield stress than the CCPI:OP=1:40 system. It is speculated that this may occur because of improved dispersion stability at higher polymer concentrations.

2) Apparent Viscosity Test

Apparent viscosity (η_{app}), which is derived by the ratio between shear stress and shear rate, decreases with increasing shear rate and is shown in Figure 7, 8 and 9. The phenomenon of the decreasing apparent viscosity with increasing shear rate is known as shear-thinning behavior and it is due to the presence of micron-sized particles. At higher shear rates the apparent viscosity decreases, ultimately reaching a constant value. This shear-thinning phenomenon can be represented by the following equation:

$$\eta_{app} \propto \dot{\gamma}^{-\Delta} \tag{5}$$

where Δ is a constant, which may vary slightly with different field. The analytical and experimental results show that the range of Δ is from 0.68 to 0.93. magnetic field investigated.

2.2 MR Damper Analysis, Design, Fabrication and Experimental Study

Introduction

Cross-country performance of military off-road vehicles is a key element for success in military operations. Cross-country performance can be determined by using different methods. Maximum velocity and harshness of pitch and roll motions of vehicles under off-road conditions can be used as parameters determining the cross-country performance [14]. Therefore, the suspension system of these kinds of vehicles is closely related with the cross-country performance characteristics on rough terrain.

Passive suspension systems using passive elements such as helical springs and viscous dampers are designed to meet the requirements of conflicting demands, i.e., ride comfort, road holding and handling. Active suspensions are one of the solutions used to improve the performance of the suspension system. Studies related to active suspension systems started in the 1960's [15]. They can improve the ride quality, road holding and handling characteristics significantly by controlling the damper force compared to the passive suspensions [15,16,17]. Experimental results conclude that the power absorbed by the driver is reduced by 95% and a 65% reduction is obtained in peak sprung mass acceleration by using an active suspension system for the HMMWV [16]. However, complexity of the design, high power requirements, weight and cost are the disadvantages of using active suspensions. Semi-active dampers are devices combining

the advantages of passive and active dampers. Indeed, they are much simpler than active dampers and have better performance characteristics than passive dampers therefore, there are many researches, started by the early 1970's, studying semi-active dampers [14,18,19,20]. Experimental studies done on the US Army M551 tank show that the power absorbed by the driver is reduced by 43% by consuming virtually no power with respect to the active suspension systems [20]. Many of the studies on semi-active suspension systems consider dampers using electro-hydraulic valves but recently magneto-rheological fluid (MRF) dampers have also been studied for military and passenger ground vehicles [21,22,23]. Experimental studies done on the HMMWV prove that the power absorbed by the driver is reduced up to 70% [21]. MRF dampers do not need any movable valve to change a force characteristic of the damper. On the other hand, they use the unique characteristic of a MR fluid; that is controllability of effective viscosity by applying an external magnetic field to valves.

Recently, an MRF damper for a High Mobility Multi-Purpose Wheeled Vehicle (HMMWV) has been developed at the Composite and Intelligent Materials Laboratory in the Mechanical Engineering Department of the University of Nevada, Reno (UNR) [23]. This study is the benchmark for our current research. This study concluded that the force of the MRF damper can be increased by keeping the uncontrolled force the same as the original equipment manufacturer (OEM) damper for the HMMWV. However, the damper, which has been developed for that study needed some modifications in terms of its feasibility for real life applications. Force characteristics, size, and power consumption of the damper had to be optimized.

Therefore, this study is aimed toward the design, fabrication and evaluation of the performance of a new MRF damper for the HMMWV. The main objective of the new design is to develop an

MRF damper that is feasible to use for the HMMWV in terms of force characteristics, size and power consumption of the damper. Figure 10 shows three different dampers developed for the HMMWV. The new MRF HMMWV damper is on the left, and the previous MRF HMMWV damper is on the right and an OEM HMMWV damper is in the center.

A new damper is designed as a fail-safe damper i.e. the damper can supply enough damping in the case of control system or power supply failure. This phenomenon is crucial for off-road vehicles since malfunction of the control system can cause severe damages to the vehicle or passengers when a vehicle is on rough terrain unless the viscous (off-state) force of a damper is enough. To determine the off-state force, the OEM damper force is taken as a reference point, as in the previous study; however, the off-state force is not exactly matched with the OEM damper force. The off-state force is optimized by keeping it smaller than the OEM damper force; while at the same time keeping the ride and stability characteristics in safe levels. By lowering the off-state force to optimum values, the controlled force region is increased for a desirable better ride quality.

A new damper is designed to match the geometrical parameters, such as, outer diameter, extended and compressed lengths of the OEM damper. In addition to that, the new damper is designed to operate with the vehicle's battery.

Another important objective of this research is to obtain different viscous force characteristics between the rebound and the compression phases, as in the OEM viscous dampers for ground vehicles. Non-symmetric characteristic has been obtained by using two-way valves [24]. Ivers

at al. presented movable and one-way valves to obtain a non-symmetric characteristic. In our study, instead of changing the piston geometry for different flow directions, shims are used to provide the non-symmetric force behavior between rebound and compression. They are very simple and inexpensive to use.

MRF Damper Analysis and Design

Figure 11 illustrates the inside of the MRF damper. The proposed MRF damper is not a through shaft damper, therefore, an accumulator is connected to volume 2 to compensate for the volume change due to the movement of the shaft. The force characteristic of a damper is directly related with the pressure drop through the piston. Piston geometric parameters, i.e., the sizes and locations of orifices and electromagnet, determine the pressure drop through the piston. Therefore, every component of the piston geometry design is explained in detail in the following sections. First, fluid flow analysis through the piston is formulated, then, pressure drops and force calculations are explained.

a) Flow rate through the piston

The mass flow rate for a control volume containing incompressible fluid can be written as [25]:

$$\frac{d}{dt}(m) = \frac{d}{dt}(\rho \cdot V) = \rho_i \cdot Q_i - \rho_o \cdot Q_o = \rho \cdot (Q_i - Q_o) \tag{6}$$

where m is the mass of the fluid inside the control volume, ρ is the fluid density, taken as constant for inlet and outlet conditions, V is volume, Q is volume flow rate, and subscripts *i* and *o* represent inlet and outlet, respectively. Rebound and compression phases of a cycle are considered below.

Rebound phase,

Equation (6) is applied to the volume 1 (V_1) of the damper. For the rebound phase $Q_i = 0$; therefore, Equation 6 reduces to,

$$\frac{dV_1}{dt} = -Q_0 \tag{7}$$

The geometric relations within the damper yield,

$$V_1 = (L_1 - u) \cdot (A_p - A_s)$$

$$\frac{dV_1}{dt} = -\dot{u} \cdot (A_p - A_s) \tag{8}$$

where u is the piston displacement, $\dot{u}$ is the piston velocity, A_p is the cross sectional area of the piston and A_s is the cross sectional area of the shaft. Then, the flow equation for the rebound case can be derived by using Equations (7) and (8),

$$Q = (A_p - A_s) \cdot \dot{u} \tag{9}$$

Compression phase

The same flow rate, in Equation (9) can be derived for the compression case using the same procedure above. Therefore, the flow rate formulation for rebound or compression can be used as a general flow rate formulation.

b) Pressure Drop Equations

Pressure drop due to the viscosity of the fluid obtained assuming an incompressible Newtonian flow through the orifices. In the new MRF damper design, a gap between two parallel fixed disks with radial flow is used as the main MR valve in addition to these common orifices as

viscous channels. Figure 12 shows the cross-sectional view of the piston in which all orifices can be seen.

The MR valve is created when an external magnetic field is applied to control the flow behavior in a channel. The effect of material properties and the geometry on the magnetic filed are examined to enhance the controllable pressure drop due to MR effect. Parallel disk type MR orifice, which can be seen in the Figure 13, used in this design also introduces uncontrollable viscous pressure drop. This pressure drop together with the other viscous channels creates the minimum damping force in the inactivated state (off state), which is the fail-safe criteria adopted for this design.

b.1) Pressure Drop due to the MR Effect

The flow rate equation between the fixed rectangular parallel plates is derived and is converted to the flow rate equation between two parallel fixed disks. The following equation describes the flow between the fixed rectangular parallel plates considering the Bingham Plastic model [26],

$$(\frac{dp}{dx})^3 - [\frac{12 \cdot Q \cdot \mu}{b \cdot h^3} + 3 \cdot \frac{\tau_y}{h}] \cdot (\frac{dp}{dx})^2 + 4 \cdot (\frac{\tau_y}{h})^3 = 0 \qquad (10)$$

where $\frac{dp}{dx}$ is the pressure drop per unit length of plates, b is the width of the plates, h is the gap thickness between the plates and τ_y is the controllable yield stress of the fluid. From equation (10) one has, [27],

$$\frac{dp}{dx} = 2.85 \cdot \frac{\tau_y}{h} + \frac{12 \cdot \mu \cdot Q}{b \cdot h^3} \qquad (11)$$

To apply the above formula for the flow between two parallel fixed disks, the following correspondences of symbols are made [28,29]

$$b \rightarrow 2 \cdot \pi \cdot r$$
$$\frac{dp}{dx} \rightarrow \frac{dp}{dr}$$

Then the radial pressure gradient is obtained as,

$$\frac{dp}{dr} = 2.85 \cdot \frac{\tau_y}{h} + \frac{6 \cdot \mu \cdot Q}{\pi \cdot r \cdot h^3} \tag{12}$$

Integrating Equation (12) gives

$$\Delta P_{disk\,mr} = 2.85 \cdot \frac{\tau_y}{h} \cdot (r_2 - r_1) \tag{13}$$

$$\Delta P_{disk_{vis}} = \frac{6 \cdot \mu \cdot Q}{\pi \cdot h^3} \cdot \ln(\frac{r_2}{r_1}) \tag{14}$$

where r_2 and r_1 are the outer and inner radius of the disks.

b.2) Pressure Drop Through the Viscous Orifices

Circular cross section

The pressure drop in the cylindrical viscous channel for the flow of an incompressible Newtonian fluid is well known and it is given as

$$\Delta P_{vis1} = \frac{128 \cdot \mu \cdot Q}{\pi \cdot D^4} \cdot L \tag{15}$$

where D is diameter of the orifice, L is length of the orifice, Q is flow through the orifice and μ is viscosity of the fluid.

Rectangular cross section

For flow in rectangular cross section, one has

$$\Delta P_{vis2} = \frac{12 \cdot \mu \cdot Q}{w \cdot h^3} \cdot L \tag{16}$$

where w is width of the channel and h is height of the channel. The gap between the two cylinders produces

$$\Delta P_{vis3} = \frac{2 \cdot \mu \cdot Q}{\pi \cdot C} \cdot L \tag{17}$$

where,

$$C = \frac{r_2^4 - r_1^4}{4} - \frac{c_1}{2} \cdot (r_2^2 \cdot \ln r_2 - r_1^2 \cdot \ln r_1) + \frac{c_1}{4} \cdot (r_2^2 - r_1^2) + \frac{c_2}{2} \cdot (r_2^2 - r_1^2)$$

$$c_1 = \frac{r_1^2 - r_2^2}{\ln r_1 - \ln r_2}$$

$$c_2 = \frac{r_1^2 \cdot \ln r_2 - r_2^2 \cdot \ln r_1}{\ln r_1 - \ln r_2}$$

$r_{1:}$ radius of the inner cylinder, r_2: radius of the outer cylinder.

Therefore, the total viscous drop is obtained by combining Equations (15)-(17), as shown below:

$$\Delta P_{vis} = \Delta P_{disk_{vis}} + \Delta P_{vis1} + \Delta P_{vis2} + \Delta P_{vis3} \tag{18}$$

b.3) Pressure Drop due to the Minor Losses

Minor losses, refer to energy losses associated with miscellaneous fittings: elbows, expansions, etc. They are considered as minor losses in long pipe systems but in damper applications due to the short length of the orifices, they may become major losses [30]. Therefore, minor losses

have to be taken into account in the pressure drop calculations. The pressure drop associated with minor losses are calculated using the following formula,

$$\Delta P_m = \frac{K_L \cdot \rho \cdot V^2}{2} \tag{19}$$

where K_L is the overall minor pressure drop coefficient, ρ is the fluid density and V is the average velocity of the fluid.

b.4) Pressure Drop Due to the Shims

Shims are used in the HMMWV OEM damper in order to achieve non-symmetric force characteristics. The energy loss is greater in the rebound phase compared to the compression phase. In this research, the same method is used to achieve non-symmetrical force characteristics. Shims are only placed on the top portion of piston. The pressure drop due to the shims is assumed to be the following form:

$$\Delta P_s = C_1 \cdot V^2 + C_2 \cdot V \tag{20}$$

where C_1 and C_2 are the coefficients depending on the material, shape and number of shims and V is the velocity of the piston.

c) Electromagnetic Analysis

The magnetic field distribution inside the MRF damper is evaluated using ANSOFT finite element analysis (FEA) software. A three-dimensional model of the damper, which can be seen in Figure 14, is developed and Ansoft software is used for specified boundary conditions that include material properties, electromagnetic activation current, and element insulation. A relationship between electromagnet activation current and magnetic field strength is determined using this software.

The geometrical parameters optimized in the electromagnetic analysis part can be seen in Figure 15. They are the coil width, MR disk radius and MR disk thickness. Since the outer diameter of the damper is one of the design constraints, taken as the OEM damper outer diameter, coil width and MR disk radius need to be optimized in this limited space. Ansoft is used to solve different piston models with different values for the coil width and MR disk radius. A combination giving the greatest MR force is selected. After optimizing the coil width and MR disk radius values, the MR disk thickness is determined. Different MR disk thickness values give different magnetic flux density values inside the MR channel; Figure 16 shows the relation obtained between magnetic flux density and MR disk thickness. Based on the results presented in Figure 16, a thickness between 1-3 mm, is selected as a desired value of MR disk thickness. Table 1 shows all the parameters related with the electromagnetic analysis.

c.3) Electromagnetic Analysis Results

Using the final design parameters, electromagnetic analysis is performed for different electrical current inputs. Figure 17 shows the magnetic flux density values inside the MR channel as a function electrical current input. Theoretically, 0.65 T is achieved inside of the MR channel and it is uniformly distributed due to the symmetry and the disk type MR channel. Figure 18 shows the distribution of magnetic field inside the MR channel. In addition to this, the magnetic flux density vectors on the MR disk surface, as well as, the mesh used in the solution can be seen in Figure 19.

By using the dimensions obtained from the electromagnetic analysis, electromagnet coil resistance is 3.5 ohm. which is a low resistance. This allows to apply currents as high as 2 or 3 Amp and therefore, a low electrical power.

d.4) Damper Force

Force of the damper can be written as

$$Fd = P_1 \cdot A_1 - P_2 \cdot A_2 + F_f \cdot sign(\dot{u}) \tag{21}$$

where F_f is the seal friction force

$$\left|P_1 - P_2\right| = \Delta P_{disk_{mr}} + (P_{r_1} - P_{r_2}) + \Delta P_{vis} + \Delta P_m \tag{22}$$

In determining P_2, nitrogen gas inside of the accumulator is assumed as an ideal gas. This provides:

$$P_o \cdot V_o{}^{\gamma} = P_a \cdot V_a{}^{\gamma} \tag{23}$$

where P_o is initial pressure of the accumulator, V_o is initial volume of the accumulator, P_a is final pressure of the accumulator, V_a is final volume of the accumulator, γ is coefficient of thermal expansion (1.4~1.7 for adiabatic expansion). In this study, 1.4 is used for thermal expansion coefficient in this study.

In addition, conservation of mass for an incompressible fluid yields:

$$V_a - V_o = A_s \cdot u \tag{24}$$

where As is cross sectional area of the shaft. Combining Equations (23) and (24) gives;

$$P_a = P_o \cdot \left(\frac{V_o}{V_o + A_s \cdot u \cdot sign(\dot{u})}\right)^{\gamma}$$

Since it is assumed that P_2=P_a, using the Equation (22) the damper force can be expressed as by:

$$F_d = (\Delta P_{vis} + \Delta P_{\min or} + \Delta P_{disk_{mr}} \cdot sign(\dot{u}) + P_a) \cdot A_1 - P_a \cdot A_2 + F_f \cdot sign(\dot{u}) \qquad (25)$$

Result and Discussion

Two different MRF damper dampers were designed, fabricated and tested. They are named UNR-MRD-005-1 and UNR-MRD-005-2. Characterization experiments are focused on investigating the effects of using shims inside the damper and the MR properties of the MRF on the force-displacement and force-velocity behavior of the damper. Experimental results are presented in two different sub-sections to point out these two different effects separately. After the experimental results are presented, theoretical and experimental results are compared. A comparison is made separately for the off-state and on-state cases of the MRF damper.

1. Effect of Shims

The test results of the MRF damper with and without shims are presented. Four different shaped shims are used to analyze the effect of using shims. From the test results, it is concluded that shims do not change the compression force but they increase the rebound force of the damper.

Experimental Results of the UNR-MRD-005-1

Figure 20 and Figure 22 (a) shows the effect of using shims on UNR-MRD-005-1 force characteristics. Although compression force almost remains constant, rebound force increases 200% when shims are used.

Experimental Results of the UNR-MRD-005-2

Figure 21 and Figure 22 (b) shows the effect of using shims on UNR-MRD-005-2 force characteristics. Compression force remains constant for UNR-MRD-005-2. On the other hand,

increase in the rebound force is less for UNR-MRD-005-2. Therefore it is concluded that, effect of shims is a function of fluid velocity.

2. MR Effect on the Damper Force Characteristics

In this section, force-displacement and force-velocity behaviors of the UNR-MRD-005-2 with an applied current to the damper are analyzed. The OEM damper force characteristics with the off-state force characteristics of the UNR-MRD-005-2 are compared. Dynamic force range of the damper is also presented. From the experimental results it is concluded that the activation of the damper with electrical current increases the force of the damper both in rebound and compression phases. Dynamic force range of the damper can be seen in Figure 25. For the rebound phase, up to 16 times higher forces can be obtained from the damper with a 3.14 cm/s piston velocity. For the compression phase, 20 times higher force can be obtained from the damper with the same piston velocity. The ratio of the full on-state force to off-state force decreases when the piston velocity increases.

3. Theoretical Estimations

Theoretical estimations are obtained from the fluid mechanics and electro-magnetic based model. Fluid mechanics based model estimations are analyzed separately from electro-magnetic analysis model. For this reason, viscous (off-state) force estimations and on-state force (summation of the viscous and MR force) are compared separately and presented in Figure 26 and 27, respectively. From the comparison, it is concluded that, the theoretical estimations are in a good agreement with the experimental results. Deviation from the experimental results is mainly due to the air inside of the damper.

Conclusions

The second generation HMMWV MRF damper is improved with respect to the first generation HMMWV damper in terms of many different properties. First of all, the new damper has been designed by considering the feedbacks coming from the full-scale quarter HMMWV model. Therefore, it has been proved that the new HMMWV MRF damper is a fail-safe damper and gives better ride quality with respect to the HMMWV OEM damper in the full-scale quarter HMMWV test setup. Second, as a first time in the literature, shims are used in an MRF damper. They are used to achieve a non-symmetrical force characteristic between the rebound and compression phases. It is concluded that, for this specific piston and shims geometry, the rebound force can be increased while keeping the compression force same by using shims. Therefore, one can produce non-symmetrical force characteristics by using shims. Third, the size of the new damper is reduced down tremendously. The new damper fits inside the original HMMWV suspension spring. Therefore, this damper can be used in the real life applications. This improvement is established by using a more efficient MR orifice, which is a disk type orifice, created by using the gap between two fixed cylinders. Fourth, the maximum power consumption of the new MRF damper is only 31.5 W, which is a very small amount of power consumption for vehicle applications. For the first generation damper, it was 178 W. This result is closely related with the applicability of the new damper for the real life applications as well. This great improvement is also directly related with using a disk type MR orifice. Lastly, theoretical estimations are in good agreement with the experimental results.

2.3. Full-Scale Study of Quarter-HMMWV-Model

Introduction

The design of a vehicle suspension system requires a compromise between vehicle handling and passenger comfort. Vehicle suspension systems supports the weight of the vehicle, provide directional control during handling maneuvers and should have the ability to decrease the vibration subjected to passengers and payload created by road disturbances. A conventional vehicle suspension system usually consists of a spring and a damper. The level of ride quality is determined by the amount of energy dissipation by the damper per cycle and the amount of energy stored and released by the spring. A large amount of energy dissipation usually causes harsh or uncomfortable ride, although it is beneficial for off-road driving. Controllable suspension systems are considered to be a way of minimizing the compromise between the ride quality and the handling of the vehicle. The characteristics of a controllable suspension system can be adjusted on demand either automatically or manually for any given road profile.

Theoretical Modeling

A two DOF quarter car model is used to study the performance of the dampers as shown in Figure 28. The vehicle mass with passengers is represented by sprung mass *ms* and the masses of the suspension components and the wheel are represented by an unsprung mass *mu*. The independent motion of the sprung mass is the first DOF, which is called as "body bounce" and motion of the unsprung mass is the second DOF. The vertical motion of the system can be defined as x_1 and x_2, which are the displacements of sprung and unsprung mass, respectively. The input is defined as x_r, which is the excitation due to the road profile. The suspension spring constant is k_1 and the stiffness of the tire is k_2. The damping coefficient of the shock absorber is

described by *c*. The damping coefficient of the tire has been neglected since it has a very high stiffness value.

The equations of motion for the two DOF OEM system can be written as follows:

$$ms.\ddot{x}_1 + k_1.(x_1 - x_2) + c.(\dot{x}_1 - \dot{x}_2) = 0 \tag{26}$$

$$mu.\ddot{x}_2 - k_1.(x_1 - x_2) - c.(\dot{x}_1 - \dot{x}_2) + F = 0 \tag{27}$$

where $F = \begin{cases} k_2(x_2 - x_r) & (mu+ms)g/k_2 \geq x_2 - x_r \\ (mu+ms)g & (mu+ms)g/k_2 < x_2 - x_r \end{cases}$ is the change in the spring force from the static equilibrium condition. The equation of motion should be modified for the MRF damper case. The $c.(\dot{x}_1 - \dot{x}_2)$ term should be replaced with the controllable MRF force:

$$ms.\ddot{x}_1 + k_1.(x_1 - x_2) + F_{MRFdamper} = 0 \tag{28}$$

$$mu.\ddot{x}_2 - k_1.(x_1 - x_2) - F_{MRFdamper} + F = 0 \tag{29}$$

$$F_{MRFdamper} = ViscousForce + MRForce \tag{30}$$

The MRF damper force consists of a viscous damping force and the force due to MR fluid activation. The viscous force is present even in the absence of the magnetic field. The MR force is the controllable force component and can be varied by a control system. A control algorithm and a mathematical model should be utilized to determine the appropriate magnetic field

required to generate necessary MR force. Table 2 presents system parameters for the full-scale quarter HMMWV Model.

Control Algorithms

On-off and continuous skyhook control algorithms are utilized to control the MRF damper. In skyhook control, a fictitious damper is connected to inertial reference in the sky. Figure 29 illustrates the skyhook-controlled damper used in the quarter car model.

The control condition criteria for the on-off skyhook algorithm is the product of the absolute velocity of the sprung mass ($\dot{x}_1$) and the MRF damper relative velocity ($\dot{x}_1 - \dot{x}_2$). If $\dot{x}_1(\dot{x}_1 - \dot{x}_2)$ is greater than 0, then the pre-determined constant current (0.5 amp) is supplied to the MRF damper. On the other hand, if $\dot{x}_1(\dot{x}_1 - \dot{x}_2)$ is equal or less than 0, then no current is supplied to damper, and in this case, MRF damper has the same characteristic as the passive-off damper. The on-off skyhook control rule can be expressed, as follows:

$$F_{MR} = \begin{cases} F_c \rightarrow \dot{x}_1(\dot{x}_1 - \dot{x}_2) > 0 \\ 0 \rightarrow \dot{x}_1(\dot{x}_1 - \dot{x}_2) \leq 0 \end{cases} \tag{31}$$

Where F_c is a constant force.

In continuous skyhook control, the MR force is not switched between 0 and constant value. The MR force varies between minimum and maximum force values, which are 0 N and 3500 N, respectively, for this particular MRF damper design. The control condition criteria of continuous

skyhook is similar to on-off skyhook control, the only difference is the applied force. If $\dot{x}_1(\dot{x}_1-\dot{x}_2) > 0$, the force is proportional to sprung mass absolute velocity. For this case, the MR damper force is equal to the product of sprung mass velocity and predetermined damping coefficient (c_s), which is also known as the skyhook damping coefficient. The skyhook damping coefficient (c_s) is determined experimentally as 5000 N.s/m. If $\dot{x}_1(\dot{x}_1-\dot{x}_2)$ is equal to or less than 0, the MR damper force changes depending on the MRF damper velocity ($\dot{x}_1-\dot{x}_2$). The continuous skyhook control rule can be expressed as follows:

$$F_{MRFdamper} = \begin{cases} c_s.\dot{x}_1 \rightarrow \dot{x}_1(\dot{x}_1-\dot{x}_2) > 0 \quad \& \quad c_s|\dot{x}_1| > ViscousForce \\ ViscousForce \rightarrow Otherwise \end{cases} \tag{32}$$

Experimental Setup

A full-scale quarter car HMMWV experimental setup is constructed to study the performance of the OEM damper and the new semi-active MRF damper. An Instron 8821S servo-hydraulic system is used to provide the input road profile. The actuator of the hydraulic unit is mounted to a plate (x_r), which is exciting the masses and the suspension system shown in Figure 30.

Four identical springs are used to model the rear tire stiffness (k_2) and mounted to sprung mass (*mu*) in parallel. The springs representing the tire are not mounted to the input plate, so that the possibility of tire losing its contact can be modeled for further experimental analysis of tire hop. A steel plate has been used to represent the mass of the components located under the suspension system. The suspension system is located between the sprung and unsprung masses. The

suspension system includes the suspension spring (k_1) and the damper (c). The original HMMWV suspension spring is used with the OEM and MRF dampers. Lead blocks are used to model the sprung mass. The lead blocks are mounted to a steel plate by threaded stainless steel bars.

A simple linear slide system consisting of ball bearings and steel shafts are used to constrain the lateral motion of the setup. A load cell is located under the suspension system in order to measure the friction of the slide system. The same load cell is also used to mea rue the sprung mass. A cable extension linear variable differential transducer (LVDT) is mounted to the sprung mass in order to measure both displacement and velocity of the vehicle body. Another LVDT is mounted between sprung and unsprung mass to measure the relative displacement and velocity. The velocity data is used as a feedback to control system during MRF damper control evaluation. An accelerometer is mounted on the sprung mass to measure the absolute acceleration of the vehicle body. A National Instrument Data Acquisition System (DAQ) is used with LabVIEW software to record the data and control the MRF damper.

Experimental Results

Simple harmonic road profiles at various amplitudes and a random road profile are used in order to study the performance of the MRF and OEM dampers. The displacement and acceleration transmissibility results of sprung mass are presented for both suspension systems using the OEM and MRF dampers under simple harmonic motion. The displacement and acceleration power spectral density (PSD) of sprung mass are investigated under random input. The root mean

square (RMS) of both displacement and acceleration for the sprung mass are presented. The MRF damper experimental results are compared with the OEM damper results.

The acceleration transmissibility shown in Figure 31 includes experimental data for 1 cm peak-to-peak amplitude simple harmonic motion. From the acceleration transmissibility data, Table 3 is generated to present the percentage of peak acceleration transmissibility reduction provided by the MRF damper as compared to the OEM damper. It should be noted that the sprung mass acceleration is the critical parameter in determining vehicle ride quality. The reduction in sprung mass acceleration increases vehicle ride quality.

The acceleration transmissibility results indicate that the ride quality of the quarter car model vehicle can be improved by utilizing skyhook controlled MRF dampers. In addition to this acceleration reduction, the MRF suspension system also offers fail-safe performance, where the MRF damper functions similar to the passive OEM damper in case of a control system malfunction.

A MRF suspension system using both on-off skyhook and continuous skyhook control has very significant acceleration reductions under simple harmonic road inputs.

Figure 32 shows the displacement transmissibility graphs of sprung mass for OEM damper and MRF damper suspension system. The displacement transmissibility behavior is very similar to the acceleration response. Based on these results, a continuous skyhook controlled MRF damper suspension system out performs one with skyhook on-off control. The reason is simply the

variable controllability range of the MR force between the maximum and minimum operating points of the MRF damper under continuous skyhook control offer more adjustability to the suspension system as compared to the on-off control strategy. Table 4 presents the displacement transmissibility reduction of sprung mass for the MRF damper system as compared to the OEM damper suspension system.

The random input is generated by MATLAB software by using the following relation [31]:

$$x + \rho V \dot{x} = V W_m \tag{33}$$

Here x and $\dot{x}$ are displacement and the velocity of the random input, respectively, ρ is the road roughness parameter, W_m is the white noise that is proportional to velocity of the vehicle V, and roughness of the road.

The velocity of the vehicle is selected as 64.5 km/h (40 mph) and the road roughness is 0.45 m^{-1}. The displacement power spectral density (PSD) of the road profile is presented in Figure 33. Figure 34 presents the acceleration PSD of the sprung mass for the random motion input. Based on the results shown in Figure 35, the ride quality is improved by 8% utilizing MRF damper with continuous skyhook control. In addition, vehicle body acceleration does not increase in case of a control system failure.

Figure 36 shows the displacement PSD of sprung mass under random motion input. Based on Figure 37, a sprung mass displacement reduction of 14% can be created by the MRF damper system using continuous skyhook control. The MR fluid damper with on-off skyhook control also exhibits better results than OEM damper for displacement PSD response. There is no

increase in displacement for passive-off case. The damper is considered to be fail-safe and provides displacement reduction with or without a control system.

3. LIST OF PUBLICATIONS

Published

1. Gordaninejad, F. and Kelso, S. P., “Magneto-Rheological Fluid Device,” U.S. Patent No. 6,471,018 B1, 2002.

2. Fuchs, A., Xin, M., Gordaninejad, F., Wang, X., Hitchcock, G., Gecol, H., Evrensel, C., and Korol, G., "Development and Characterization of Hydrocarbon Polyol Polyurethane and Silicone Magnetorheological Polymeric Gels," *Journal of Applied Polymer Science*, Vol. 92, issue 2, pp. 1176-1182, 2004.

3. Dogruer, U., Gordaninejad, F., and Evrensel, C., "A Magneto-Rheological Fluid Damper for High-Mobility Multi-Purpose Wheeled Vehicle (HMMWV)," *Damping and Isolation, Proceedings of SPIE Conference on Smart Materials and Structures,* Ed. Kon-Well Wang, Vol. 5386, pp. 195-203, 2004.

4. Karakas, S., Gordaninejad, F., Evrensel, C., Yeo, M-S, Liu, Y., and Sahin, H., "Control of a Quarter HMMWV Suspension System Using a Magneto-rheological Fluid Damper," *Damping and Isolation, Proceedings of SPIE Conference on Smart Materials and Structures,* Ed. Kon-Well Wang, Vol. 5386, pp. 204-213, 2004.

5. Liu, Y., Gordaninejad, F., Evrensel, C., Karakas, S., and Dogruer, U., "Experimental Study on Fuzzy Skyhook Control of a Vehicle Suspension System Using a Magneto-Rheological Fluid Damper, " *Industrial and Commercial Applications of Smart Structures Technologies, Proceedings of SPIE Conference on Smart Materials and Structures,* Ed. by Jack H. Jacobs, Vol. 5388, pp. 338-347, 2004.

6. Dogruer, U., Gordaninejad, F., and Evrensel, C. A., “A New Magneto-Rheological Fluid Damper for High-Mobility Multi-purpose Wheeled Vehicle (HMMWV),” *Proceedings SPIE Smart Structures and Materials Conference*, *Damping and Isolation*, Ed. By A. S. Agnes and K-W Wang, Vol. 5052, pp.198-206, 2003.

7. Liu, Y., Gordaninejad, F., Evrensel, C. A., Dogruer, U., Yeo, M-S , Karakas, E. S., and Fuchs, A., “Temperature Dependent Skyhook Control of HMMWV Suspension Using a Fail-Safe Magneto-Rheological Damper,” *Proceedings SPIE Smart Structures and Materials Conference*, *Industrial and Commercial Applications*, Ed. by E. H. Anderson, Vol. 5054, pp. 332-340, 2003.

8. Karakas, E. S., Gordaninejad, F., Evrensel, C. A., Yeo, M-S, and Liu, Y., “Study of A Quarter Model HMMWV Suspension System Using A Magneto-Rheological Fluid Damper,” *Proceedings SPIE Smart Structures and Materials Conference, Smart Structures and Integrated Systems,* Ed. By A. M., Baz, Vol. 5056, pp.506-513, 2003.

9. Wang, X. and Gordaninejad, F., "Dynamic Modeling of Semi-Active ER/MR Fluid Dampers," *Damping and Isolation, Proceedings of SPIE Conference on Smart Materials and Structures,* Ed. Daniel J. Inman, Vol. 4331, pp. 82-91, 2001.

Submissions to Journals

1. Liu, Y, Gordaninejad, F., Dogruer, U., and Evrensel, C. A., "Theoretical Study on Temperature Compensated Skyhook Control of a Vehicle Suspension Using Failsafe Magneto-Rheological Fluid Damper," submitted for publication.

2. Fuchs, A. Hu, B., Gordaninejad, F., and Evrensel, C., "Investigation and Development of Magneto-rheological Polymeric Materials for High-Payload Land Vehicles," submitted for publication.

3. Dogruer, U., Gordaninejad, F., and Evrensel, C., "A Magneto-Rheological Fluid Damper for High-Mobility Multi-Purpose Wheeled Vehicle (HMMWV)," in preparation.

4. Karakas, S., Gordaninejad, F., Evrensel, C., Yeo, M-S, Liu, Y., and Sahin, H., "Control of a Quarter HMMWV Suspension System Using a Magneto-rheological Fluid Damper," in preparation.

Reports

1. Final Progress Report, Gordaninejad, F., Fuchs, A., Dogrour, U., Karakas, S., Liu, and Y., and Evrensel, C., " A New Generation of Magneto-Rheological Dampers," Army Research Office, Interim Progress Report, August 27, 2004.

2. Interim Progress Report, Gordaninejad, F., Fuchs, A., Dogrour, U., Karakas, S., Liu, and Y., and Evrensel, C., " A New Generation of Magneto-Rheological Dampers," Army Research Office, Interim Progress Report, March 31, 2004.

3. Interim Progress Report, Gordaninejad, F., Fuchs, A., Dogrour, U., Karakas, S., Liu, and Y., Evrensel, C., " A New Generation of Magneto-Rheological Dampers," Army Research Office, Interim Progress Report, March 31, 2003.

4. Interim Progress Report, Gordaninejad, F., Fuchs, A., Dogrour, U., Karakas, S., Liu, Y., Evrensel, C., and Yeo, M-S., " A New Generation of Magneto-Rheological Dampers," Army Research Office, Interim Progress Report, December, 2001.

Presentations

1. Karakas, E. S., Gordaninejad, F., Evrensel, C., Yeo, M-S, Liu, Y., and Sahin, H., "Control of a Quarter HMMWV Suspension System using a Magneto-Rheological Fluid Damper," *Proceedings SPIE Smart Structures and Materials Conference,* in press, 2004.

2. Dogruer, U., Gordaninejad, F., and Evrensel, C., "A Magneto-Rheological Fluid Damper for High-Mobility Multi-Purpose Wheeled Vehicle (HMMWV)," *Proceedings SPIE Smart Structures and Materials Conference,* in press, 2004.

3. Liu, Y., Gordaninejad, F., Evrensel, C., Karakas, S., Dogruer, U., "Experimental Study on Fuzzy Skyhook Control of a Vehicle Suspension System using a Magneto-rheological Fluid Damper," *Proceedings SPIE Smart Structures and Materials Conference,* in press, 2004.

4. Karakas, E. S., Gordaninejad, F., Evrensel, C. A., Yeo, M. S., and Liu, Y., "An Experimental Study of HMMWV Suspension System Using a Magneto-Rheological Fluid Damper," *SPIE Conference on Smart Materials and Structures,* San Diego, California, March 2003.

5. Dogruer, U., Gordaninejad, F., Evrensel, C. A., "A Magneto-Rheological Fluid Damper for High-Mobility Multi-Purpose Wheeled Vehicle (HMMWV)," *SPIE Conference on Smart Materials and Structures,* San Diego, California, March 2003.

6. Liu, Y., Gordaninejad, F., Evrensel, C. A., Dogruer, U., Yeo, M. S., Karakas, E. S., A. Fuchs, "Temperature Dependent Skyhook Control of HMMWV suspension Using a Fail-Safe Magneto-rheological Damper," *SPIE Conference on Smart Materials and Structures,* San Diego, California, March 2003.

7. Wang, X. and Gordaninejad, F., "Lyapunov-Based Control of a Bridge Using Magneto-Rheological Fluid Dampers," *the 8th International Conference on ER/MR Fluids*, Nice, France, July 2001.

8. Wang, X. and Gordaninejad, F., "Dynamic Modeling of Semi-Active ER/MR Fluid Dampers," *SPIE Conference on Smart Materials and Structures*, Newport Beach, California, March 2001.

9. Fuchs, A., Hu, B., Gordaninejad,F., Gecol,H., Elkins,J., Evrensel, C.,"Nanostructured Magnetorheological Polymer Gels", AIChE Annual Conference, November 2003.

10. Gecol, H., Fuchs, A., Zhang, Q., Elkins, J., Gordaninejad, F., Evrensel, C.,"Modification of Magnetic Particle Surface Characteristics by Supramolecular Structure", AIChE Annual Conference, November 2003.

11. Hu,B., Fuchs,A., Gordaninejad,F., Evrensel,C.,"Magnetorheological Polymer Gels", AIChE Annual Conference, November 2003

12. Hu, B., Tibesar*, A.*, Dogruer, U., Karakas, S., Fuchs, A., Gordaninejad, F., Gecol, H., and Evrensal, C., "Magnetorheological Polymer Gels Based on High Temperature Polymers, AIChE Annual Conference, Nov. 3-8, 2002.

13. Fuchs, A., "Magnetorheological Polymer Gels", Pacific Northwest National Laboratories, Richland, WA, June 6, 2002.

14. Fuchs, A., "Development and Characterization of Nano Magnetorheological Polymer Gels", Invited Lecture, University of California, Riverside, January 10, 2002.

4. SCIENTIFIC PERSONNEL

The personnel include a multidisciplinary research group on MR materials, MRF damper system, and theoretical and experimental control. Four graduate students and a postdoctoral Fellow are partially employed by this project. In addition to the PI and Co-PI, a Mechanical Engineering Faculty member has joined the research team. The list of the project personnel is, as follows:

1. Professor Faramarz Gordaninejad, Principal Investigator, Mechanical Engineering
2. Professor Alan Fuchs, Co-Principal Investigator, Chemical Engineering
3. Professor Cahit Evrensel, Mechanical Engineering
4. Dr. Yanming Liu, Postdoctoral Fellow, Electrical Engineer
5. Mr. Huseyin Sahin, Graduate Student, Mechanical Engineering
6. Mr. Umit Dogrour, Graduate Student, Mechanical Engineering
7. Mr. Sinan Karakas, Graduate Student, Mechanical Engineering
8. Mr. Ben Hu, Graduate Student, Chemical Engineering

5. REPORT OF INVENTIONS

The following U.S. patent was published in 2002. This patent describes a novel design fora MR damper which can be used for land vehicles, specifically for HMMWV. Gordaninejad, F. and Kelso, S. P., "Magneto-Rheological Fluid Device," U.S. Patent No. 6,471,018 B1, 2002.

6. REFERENCES

1. Jolly, M.R.; Bender, J.W.; Carlson, J.D. "Properties and Applications of Commercial Magnetorheological Fluids", *SPIE 5th Annual Int. Symposium on Smart Structures and Materials*. San Diego, CA, 15 March, 1998

2. Carlson, J.D.; Jolly, M.R., "MR fluid, foam and elastomer devices," *Mechatronics*, 10, pp555-569, 2000

3. Phillips, R. W., 1969, "Engineering applications of fluids with a variable yield stress," *Ph.D. Dissertation*, University of California.

4. Park, J.H.; Chin, B.D.; Park, O.K., "Rheological Properties and Stabilization of Magnetorheological Fluids in a Water-in-Oil Emulsion, "*Journal of Colloid Interface Science* V240, pp349-354 ,2001

5. Podszun; Wolfgang (Koln, DE); Halle; Olaf (Koln, DE); Kijlstra; Johan (Leverkusen, DE); Bloodworth; Robert (Koln, DE); Wendt; Eckhard (Leverkusen, DE)., "Magnetorheological liquids, a process for producing them and their use, and a process for producing magnetizable particles coated with an organic polymer, " U.S. Pat. 5,989,447 , 1999

6. Wilson, M., Fuchs, A. and Gordaninejad, F., "Development and characterization of magnetorheological polymer gels," *Journal of Applied Polymer. Science*, V84, Issue14, pp2733-2742, 2002

7. Xin, M., "Development and characterization of novel magneto-Rheological Polymeric Gels" *M.S Thesis*, University of Nevada, Reno, 2003.

8. Carlson, J.D.; "What Makes a Good MR fluid*?" Presented at 8th International conference on Electrorheological (ER) Fluid and Magneto-rheological (MR) Suspensions*, Nice, July 9-13,2001

9. Wollny, K. Lauger, J. Huck, S., "Magneto sweep-A New Method for characterizing The Viscoelastic Properties of Magneto-Rheological Fluids" *Applied Rheology*.12, 1, pp25-31 ,2002

10. Ly, H.V., Reitich, F., Jolly. M.R., Banks, H.T., and Ito, K., "Simulations of particle dynamics in magnetorheological fluids", Journal of Computational Physics 155(1) pp160-177, 1999.

11. Ginder, J.M., Davis, L.C., and Elle, L.D., "Rheology of Magnetorheological fluid: Models and measurements," *International Journal of Modern Physics. B* 10, pp3293-3303 ,1996.

12. Ginder, J.M., Nichols, M.E., Elie, L. D., Tardiff, J. L., "Magnetorheological Elastomers: Properties and Applications, Smart Materials Technologies," Ed. By M. Wuttig, Proc. Of SPIE Vol. 3675, in press, 1999.

13. Ginder, J.M., "Rheology Controlled By Magnetic Fields," Encyclopedia of Applied Physics, Vol. 16, p487-503, 1996.

14. Hoogterp, F. B., Saxon, N. L., Schihl, P. J., "Semi-active Suspension for Military Vehicles," *Society of Automotive Engineering International Congress and Exposition,* 930847, Detroit, Michigan, March 1-5, 1993.

15. Bender, E. K., Karnopp, D., Paul, I. L., "On the Optimization of Vehicle Suspensions Using Random Process Theory," ASME, 67-TRAN-12, 1967.

16. Buckner, G. D., Schuetze, K. T., Beno, J. H., " Intelligent Feedback Linearization for Active Vehicle Suspension Control," *Journal of Dynamic Systems, Measurement, and Control,* V.12, pp 727-733, December, 2001.

17. Hoogterp, F. B., Eiler M. K., Mackie, W. J., "Active Suspension in the Automotive Industry and the Military," *Society of Automotive Engineering International Congress and Exposition,* 961037, Detroit, Michigan, February 26-29, 1996.

18. Karnopp, D., Crosby, M.J., "System for Controlling the Transmission of Energy Between Spaced Members," US Patent No. 3,807,678, 1974.

19. Karnopp, D., Crosby, M. J., Harwood, R. A., " Vibration control using semi-active force generator," *Journal of Engineering for Industry, Transactions of the ASM*E, v 96 Ser B, n 2, pp.619-626, May 1974.

20. Miller, L. R., Nobles, C. M., "The design and development of semi-active suspensions for a military tank," *Society of Automotive Engineering Future Transportation Technology Conference and Exposition,* 881133, San Francisco, California, August 8-11, 1988.

21. Gordaninejad, F., Kelso, S. P., "Fail-Safe Magneto-Rheological Fluid Dampers for Off-Highway, High-Payload Vehicles," *Journal of Intelligent Material System and Structures*, Vol. 11, No. 5, pp. 395-406, 2000.

22. www.rodmillen.com

23. Kelso, S. P., "Development and Investigation of Magneto-Rheological Fluid (MRF) Dampers for Off-Highway, High Payload Vehicles," M.S. thesis, 1999.

24. Ivers, D. E., Carlson, J. D., "Two-way Magnetorheological Fluid Valve Assembly and Devices Utilizing Same," U.S. Patent No. 6,095,486, 2000.

25. Wang, X. and Gordaninejad, F., "Dynamic Modeling of Semi-Active ER/MR Fluid Dampers," *Damping and Isolation, Proceedings of SPIE Conference on Smart Materials and Structures,* Ed. Daniel J. Inman, Vol. 4331, pp. 82-91, 2001.

26. Phillips, R W., "Engineering applications of fluids with a variable yield stress," *Ph.D. Dissertation*, University of California, 1969.

27. Wang, X., Gordaninejad, F., "Flow Analysis of Field-Controllable, Electro- and Magneto-Rheological Fluids Using Herschel-Bulkley Model," *Journal of Intelligent Materials, Systems and Structures,* Vol. 10, No. 8, Pp. 601-608, 1999.

28. Dai, G and Byron Bird, R., "Radial Flow of a Bingham Fluid Between Two Fixed Circular Disks," *Journal of Non-Newtonian Fluid Mechanics,* Vol. 8, pp. 349-355, 1981.

29. Huang, D.C., Liu, B.C. and Jiang, T.Q., "An Analytical Solution of Radial Flow of a Bingham Fluid Between Two Fixed Circular Disks," *Journal of Non-Newtonian Fluid Mechanics,* Vol. 26, pp. 143-148, 1987.

30. Dixon, J. C., "The Shock Absorber Handbook," *Society of Automotive Engineers*, February, 1999.

31. Choi, S. B., Kim, W. K., "Vibration Control of a Semi-active Suspension Featuring Electrorheogical Fluid Dampers," *Journal of Sound and Vibration*, Vol. 234(3), pp 537-546, 2000.

7. TABLES AND FIGURES

Table 1. Piston geometrical parameters determined in the electromagnet analysis.

Coil Width	8 mm
Coil Height	20 mm
Wire Gage	21
MR Disk Radius	21.5 mm
MR Disk Height	2 mm

Table 2. The System Parameters for the Full-Scale Quarter HMMWV Model.

Parameter	**Value**
Unsprung mass (*mu*)	181 kg
Sprung mass (*ms*)	818 kg
Tire spring stiffness (k_2)	463,800 N/m
Suspension spring stiffness (k_1)	163,300 N/m
Damping coefficient of OEM damper in extension	27,160 N/m/s
Damping coefficient of OEM damper in compression	9,053 N/m/s
Damping coefficient of MRF damper	Variable

Table 3. The Reduction of Sprung Mass Acceleration Transmissibility of MRF Damper Compared to the OEM Damper.

	ACCELERATION REDUCTIONS COMPARED TO OEM DAMPER
On-Off Skyhook	21%
Continuous Skyhook	28%
Passive-Off	0.90%

Table 4. The Reduction of Sprung Mass Displacement Transmissibility of the MRF Damper Compared to the OEM Damper.

MRF Damper	**DISPLACEMENT REDUCTIONS COMPARED TO OEM DAMPER**
On-Off Skyhook	13%
Continuous Skyhook	19%
Passive-Off	-9%

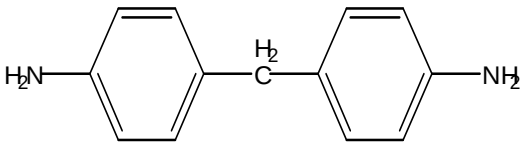

4,4’-methylenedianiline

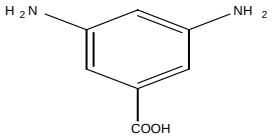

3,5-diaminobenzoic acid

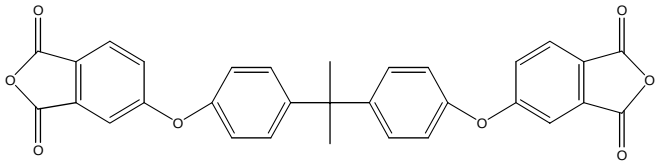

4,4’-(4,4’-isopropylidene diphenoxy)bis(phthalic anhydride)

- H_2O

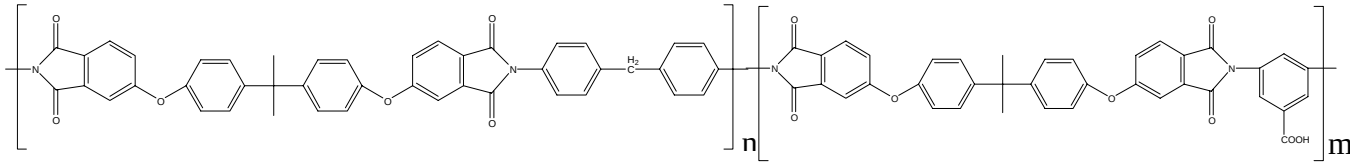

+ HO-$(CH_2)_4$-OH

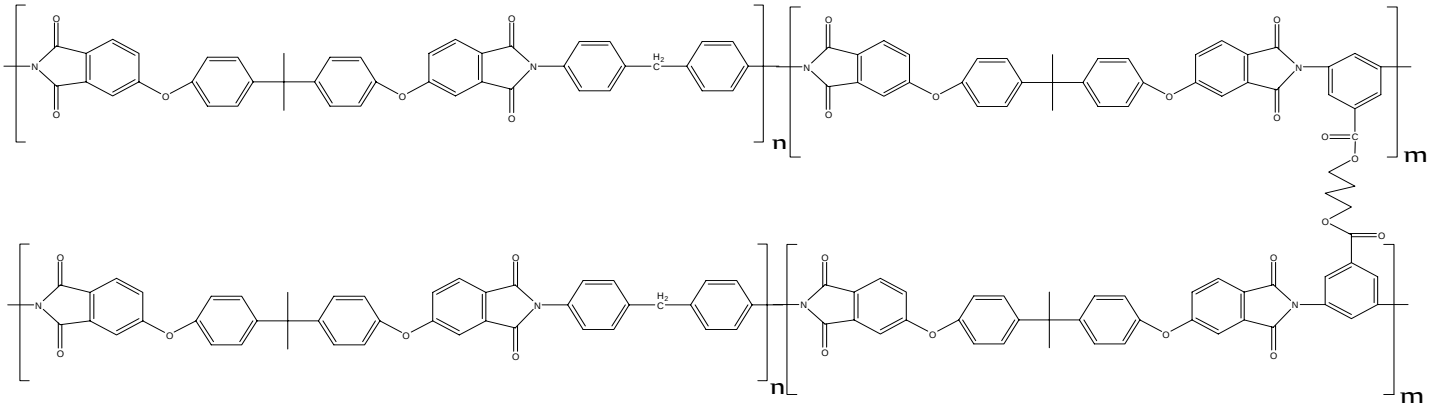

Figure 1. Synthesis of crosslinked polyimide

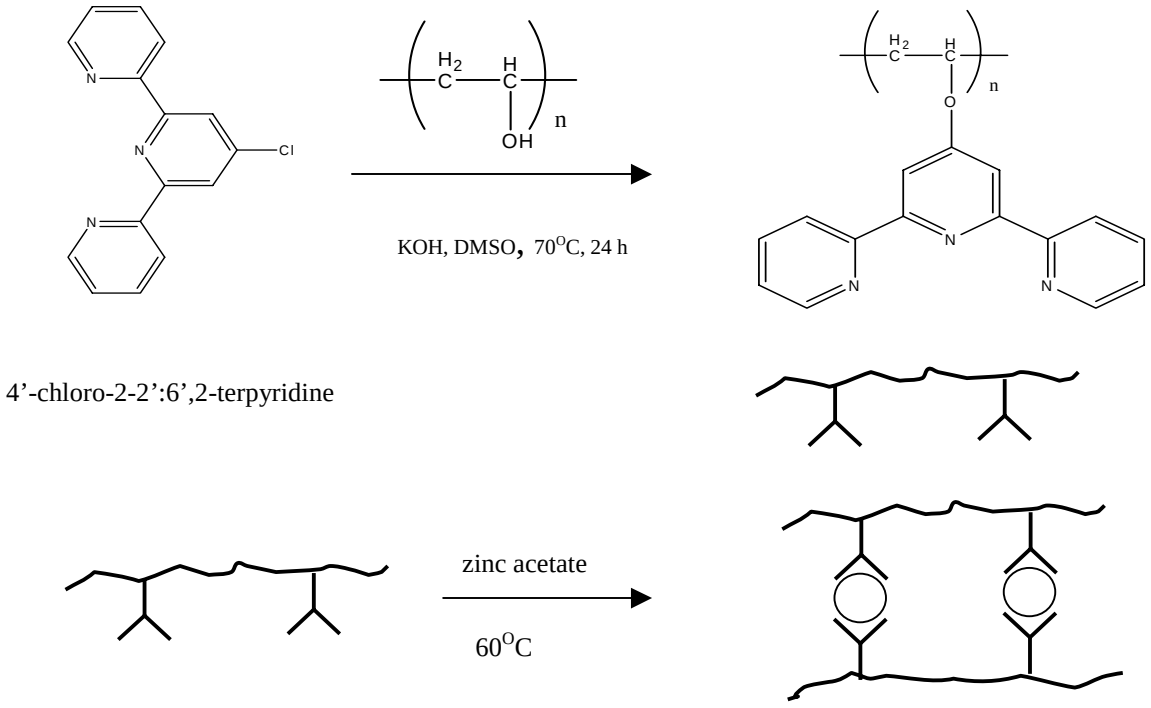

Figure 2. Synthesis of crosslinked supramolecule

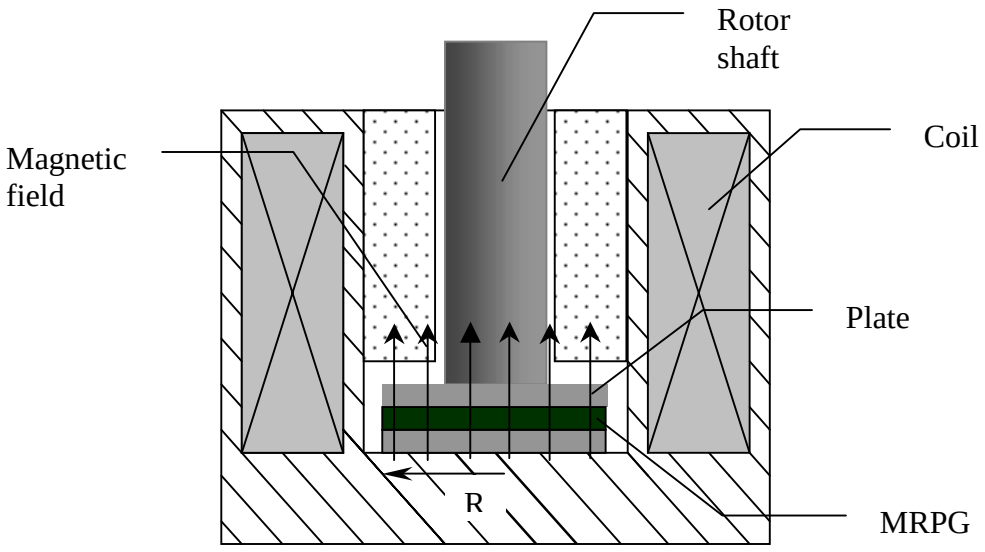

Figure 3. Schematic of the magnetorheological rheometer.

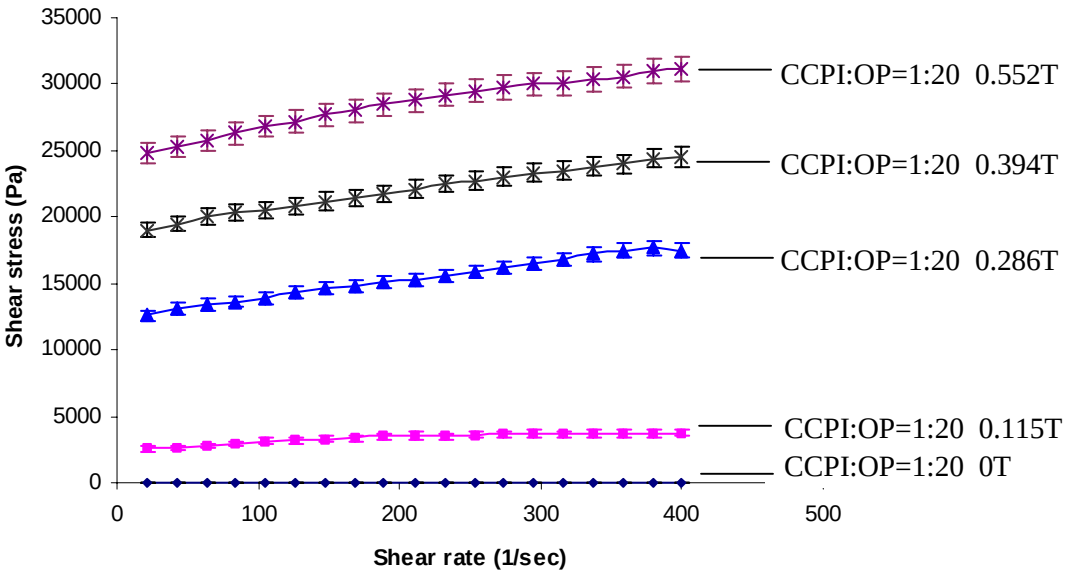

Figure 4. The dependence of shear stress of crosslinked polyimide MRPG on the shear rate at different applied magnetic field density.

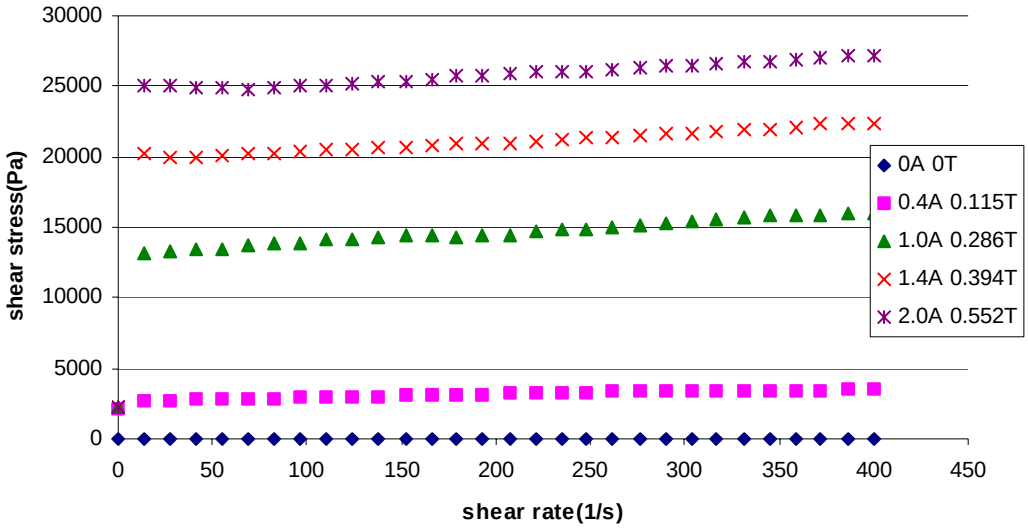

Figure 5. The dependence of shear stress of Supramolecular MRPG on the shear rate at different applied magnetic field density.

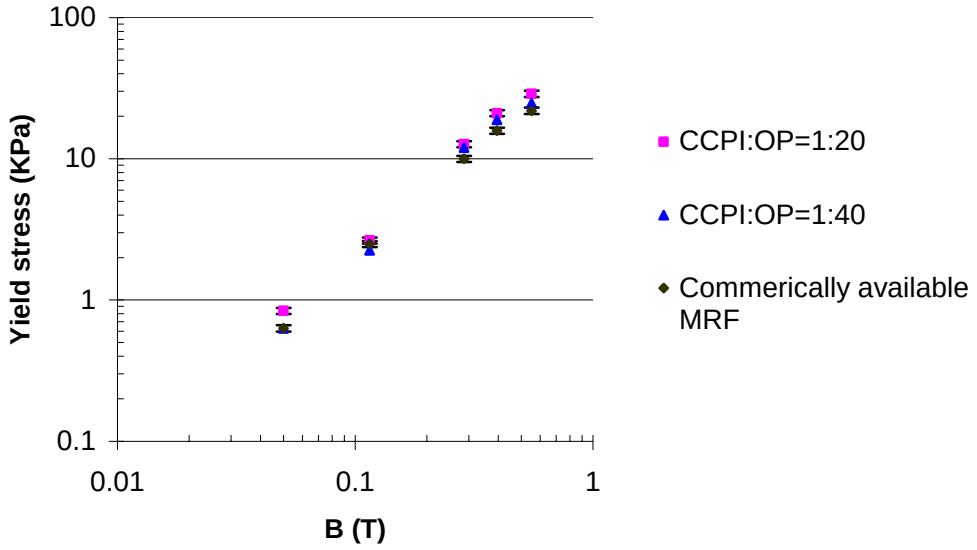

Figure 6. The dependence of dynamic yield stress of crosslinked polyimide MRPGs on the applied magnetic field.

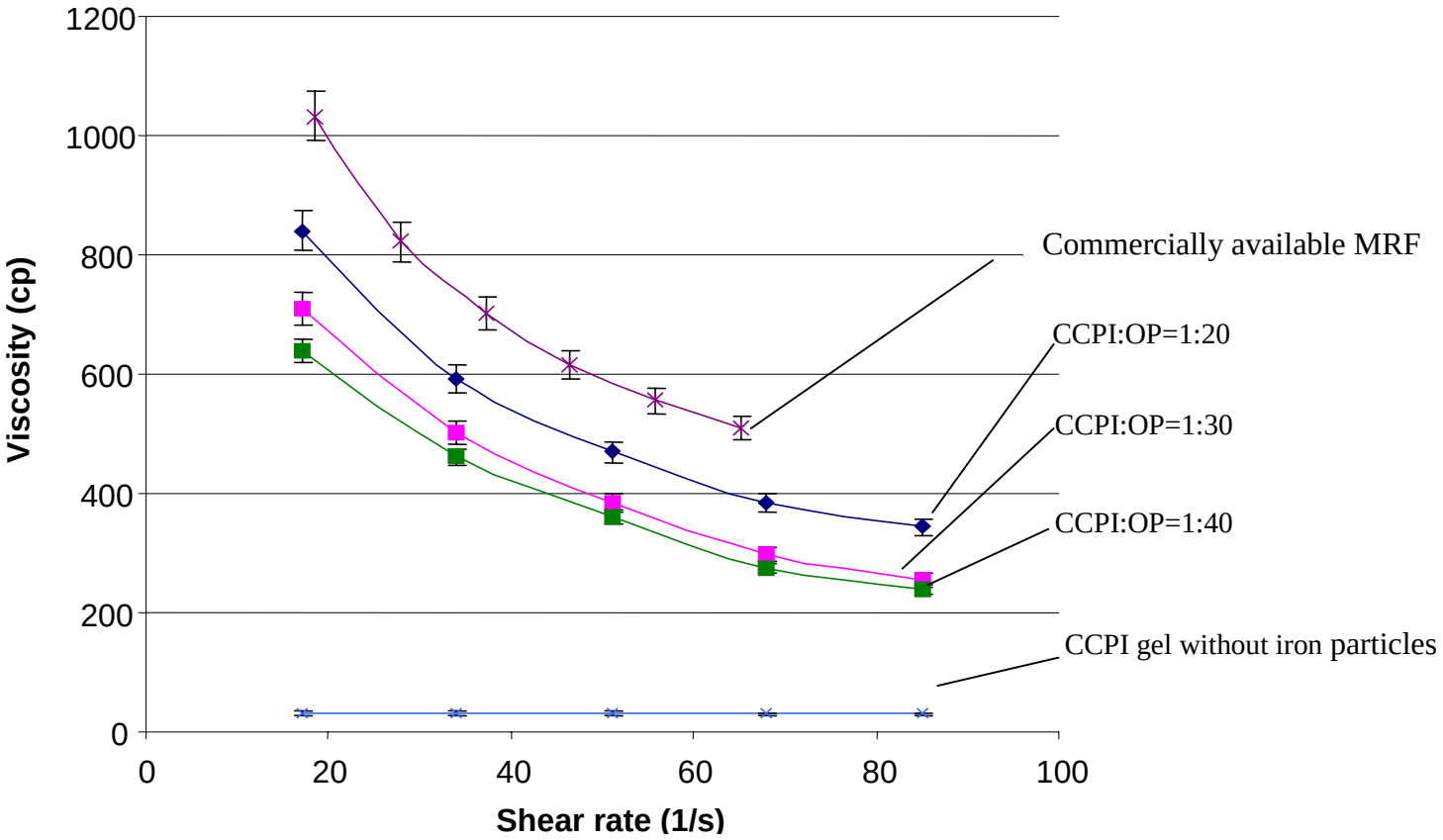

Figure 7. Off state apparent viscosity of CCPI MPRGs as a function of shear rate.

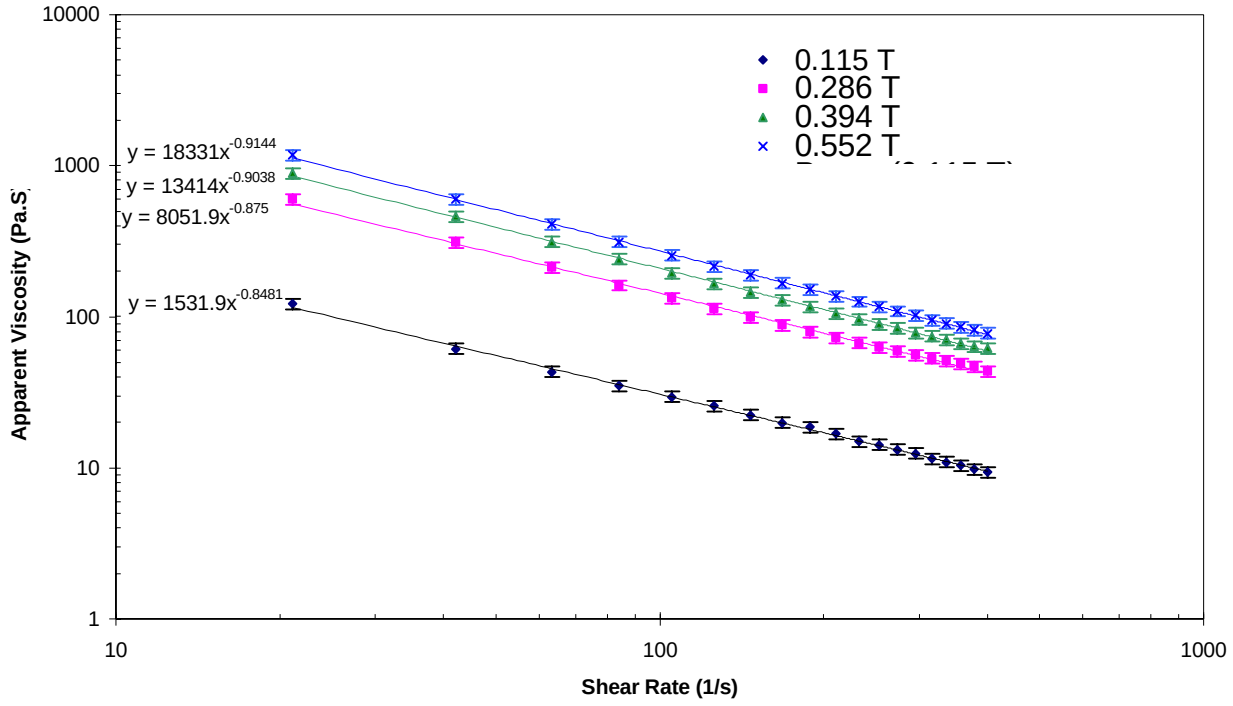

Figure 8. On-state apparent viscosity of MPRGs as a function of shear rate.

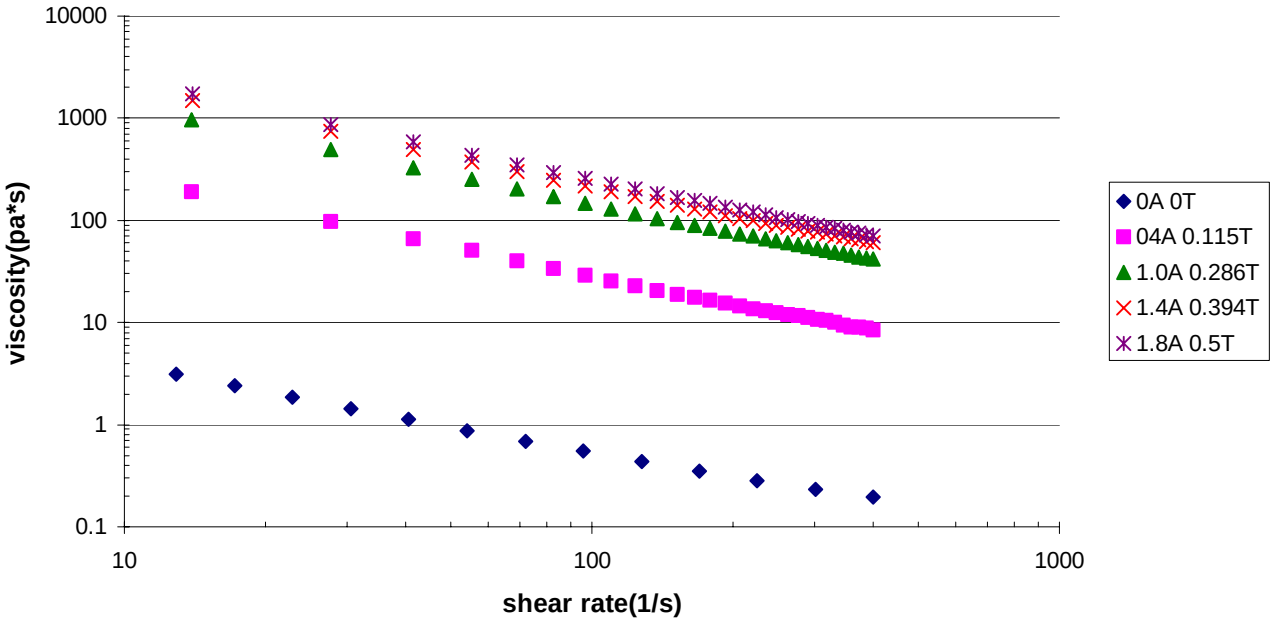

Figure 9. Log-log plot of the apparent viscosity of supramolecular MRPG versus shear rate for various magnetic fields.

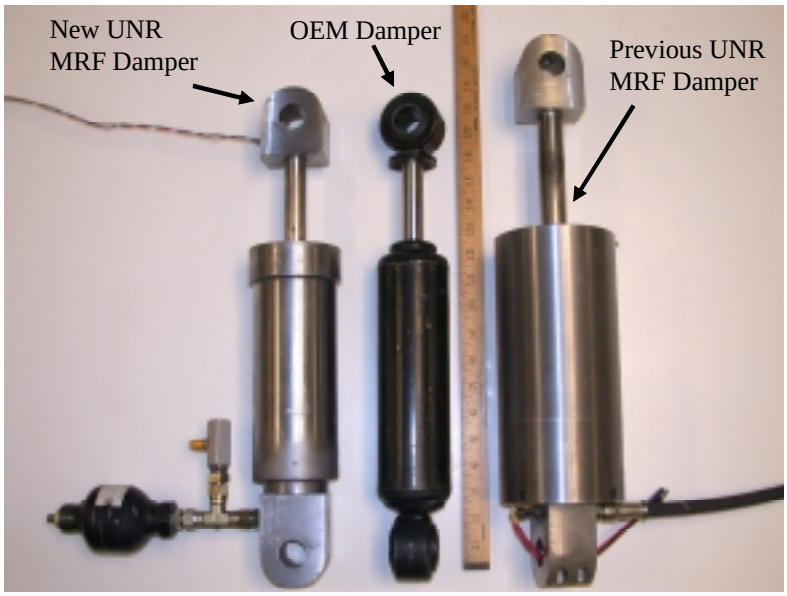

Figure 10. Two UNR HMWWV dampers and an OEM HMMWV damper.

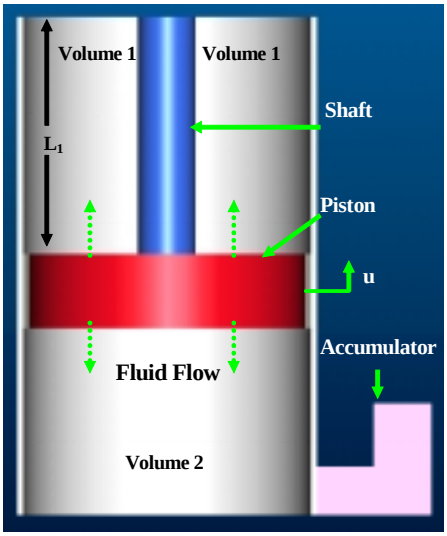

Figure 11. Schematic drawing of cross section of the damper.

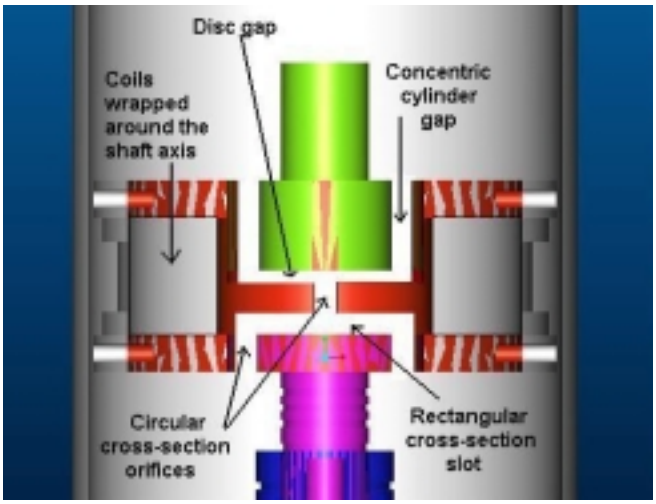

Figure 12. Cross-sectional view of the piston.

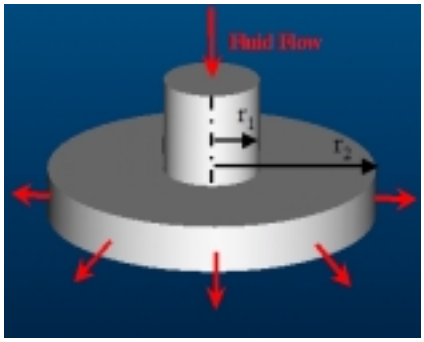

Figure 13. Schematic drawing of disk type orifice.

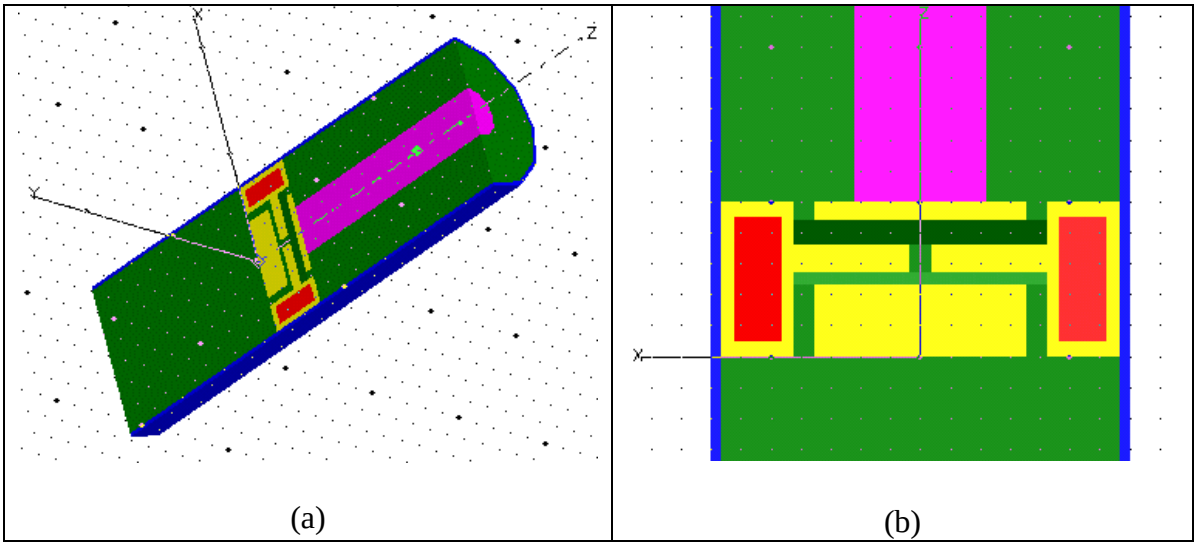

Figure 14. Cross section view of (a) the damper and (b) the piston.

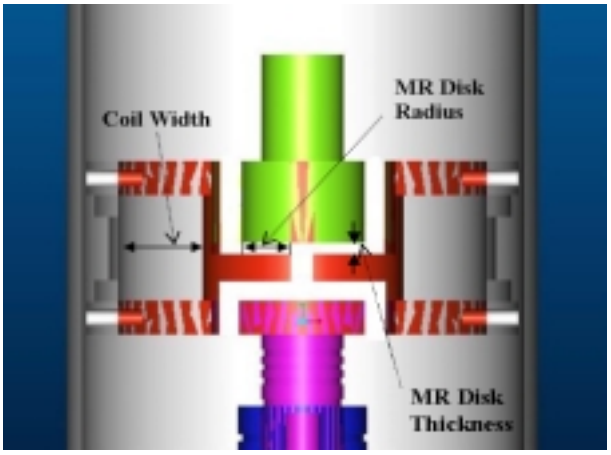

Figure 15. Geometrical parameters optimized in electromagnetic analysis.

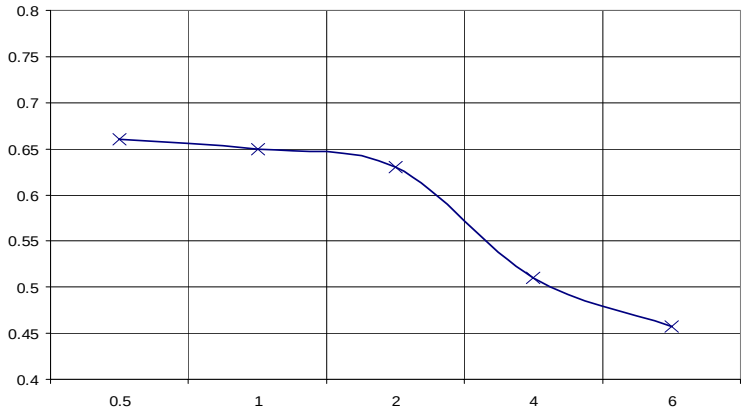

Figure 16. Magnetic flux density values inside MR disk for different MR disk thicknesses for a specific current input.

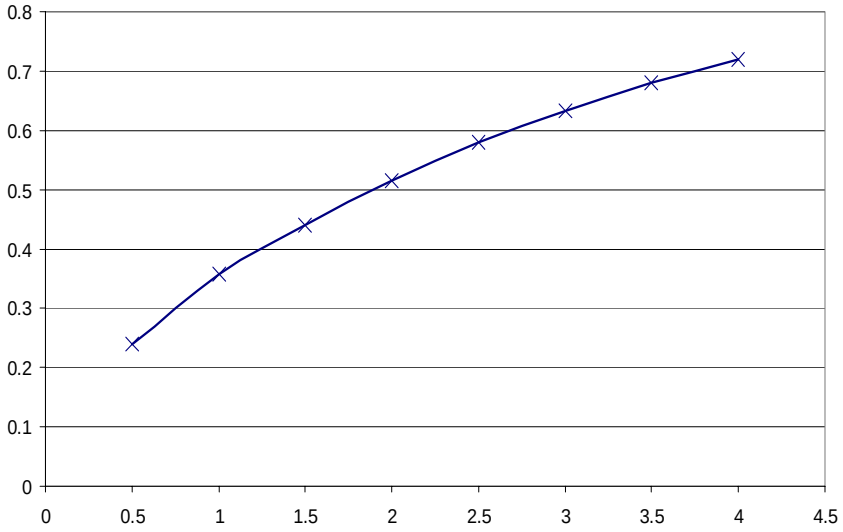

Figure 17. Magnetic flux density values inside the disk for different current values applied to the final geometry.

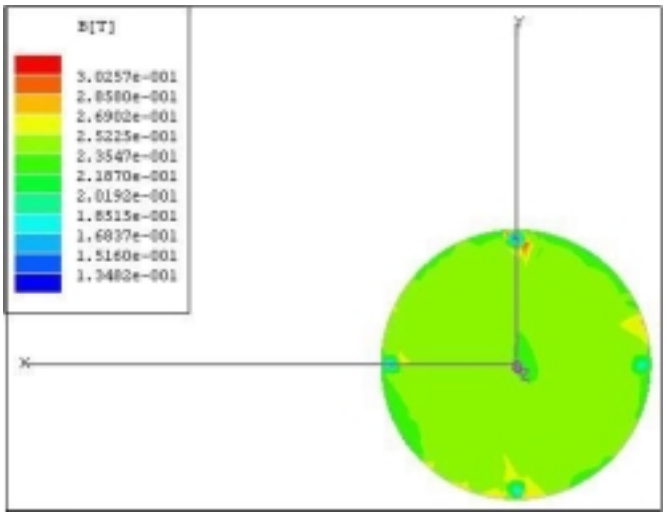

Figure 18. Distribution of magnetic field through the MR channel by 0.5 amp. electrical current applied to the final geometry.

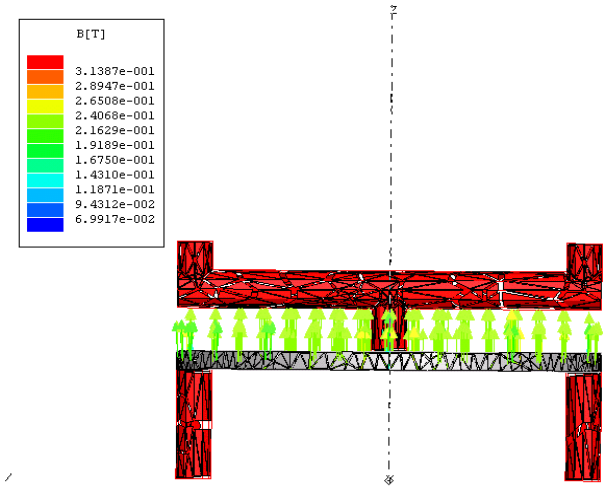

Figure 19. Magnetic flux density vectors on the meshed MR disk surface with the application of 0.5 amp. electrical current.

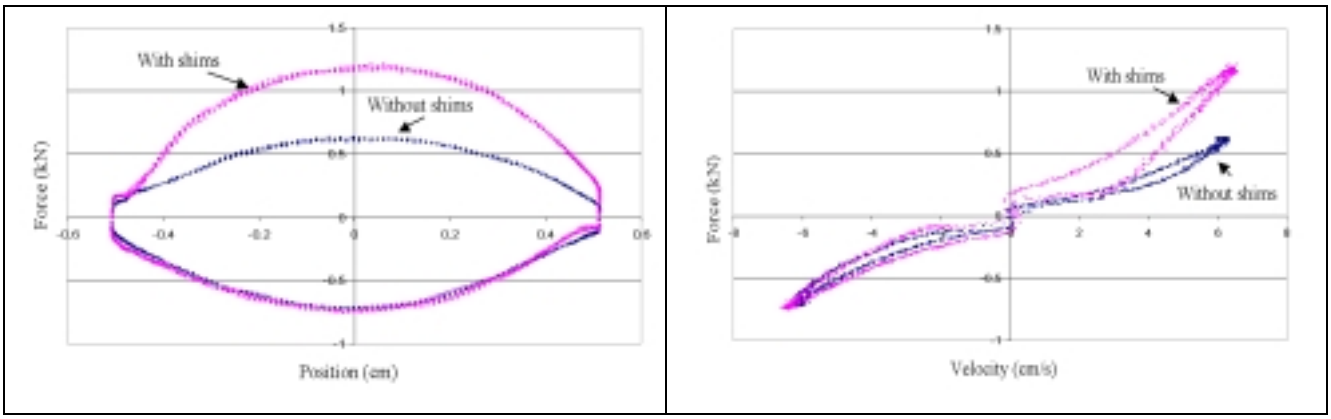

(a) (b)

Figure 20. (a) Force-displacement loop and (b) force-velocity relation of the UNR-MRD-005-1 with 2 Hz. and 1 cm. peak to peak amplitude sinusoidal input.

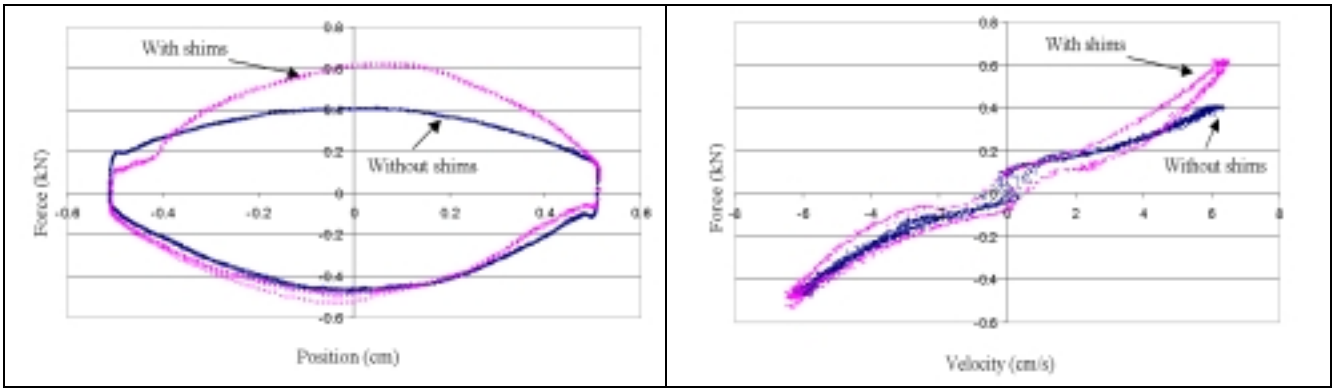

(a) (b)

Figure 21. (a) Force-displacement loop and (b) force-velocity relation of the UNR-MRD-005-2 with 2 Hz. and 1 cm. peak to peak amplitude sinusoidal input.

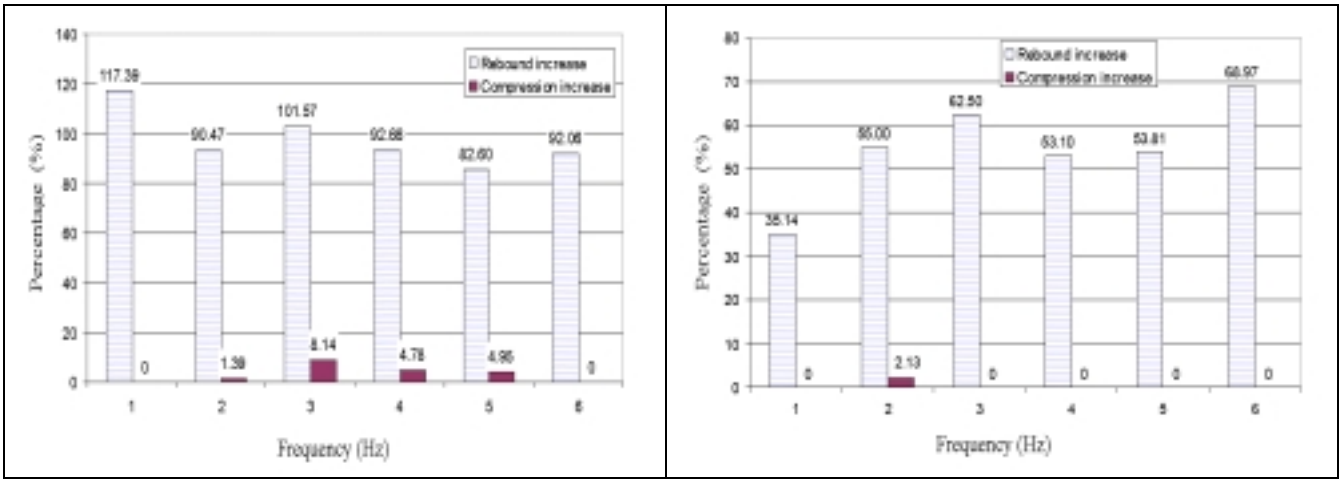

(a) (b)

Figure 22. Percentage of increase of the rebound and compression forces of the (a) UNR-MRD-005-2 and (b) UNR-MRD-005-1 due to usage of shims as a function of frequency.

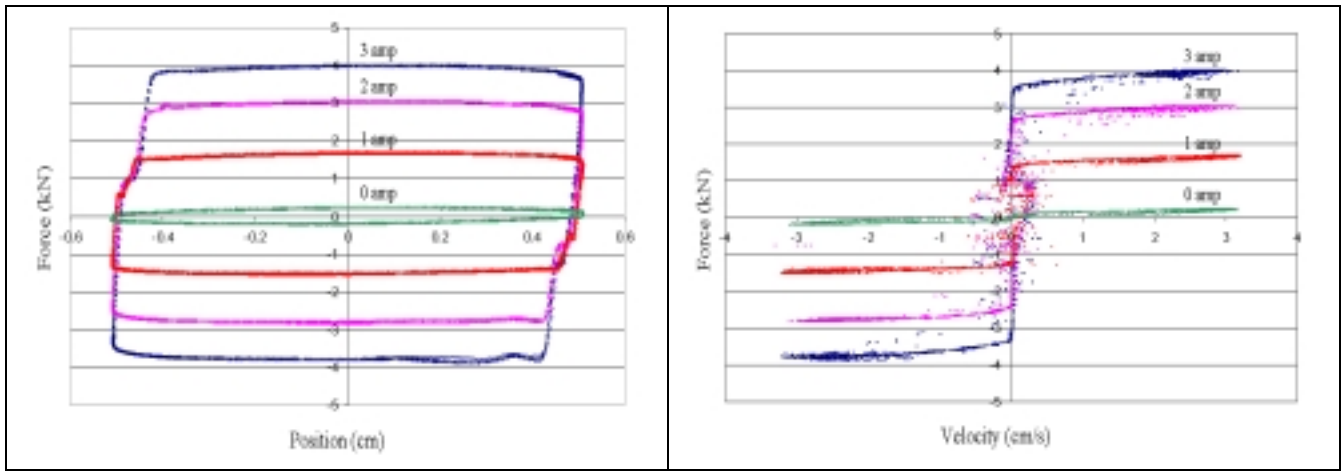

(a) (b)

Figure 23. (a) Force-displacement loop and (b) force-velocity relation of the UNR-MRD-005-2 with 1 Hz. and 1 cm. peak to peak amplitude sinusoidal and different electrical currents inputs.

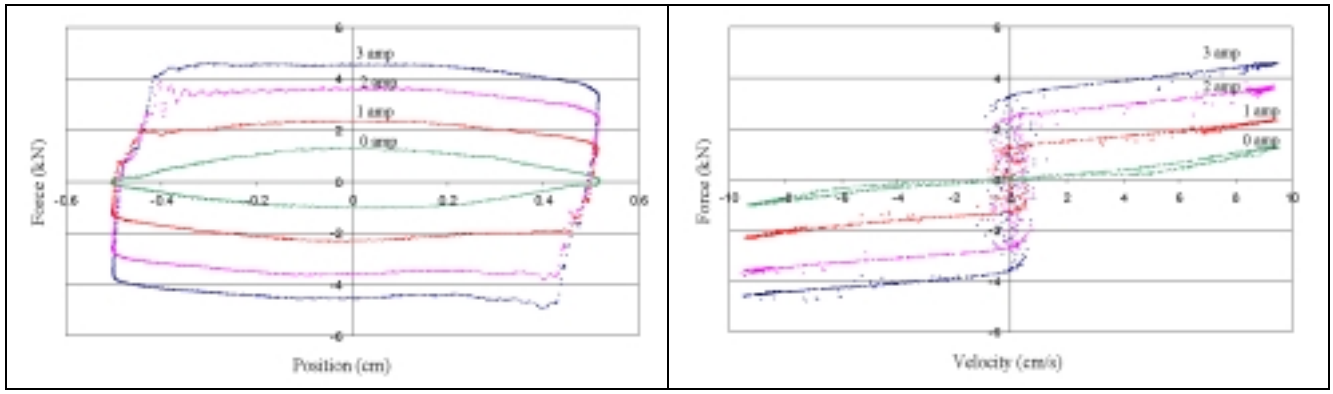

(a) (b)

Figure 24. (a) Force-displacement loop and (b) force-velocity relation of the UNR-MRD-005-2 with 3 Hz. and 1 cm. peak to peak amplitude sinusoidal and different electrical currents inputs.

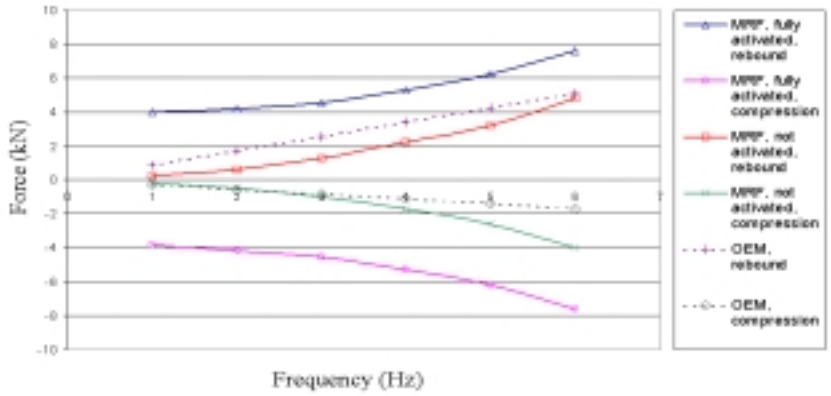

Figure 25. Comparison of the force values of the UNR-MRD-005-2 and the OEM damper as a function of frequency with 1 cm. peak to peak amplitude sinusoidal input.

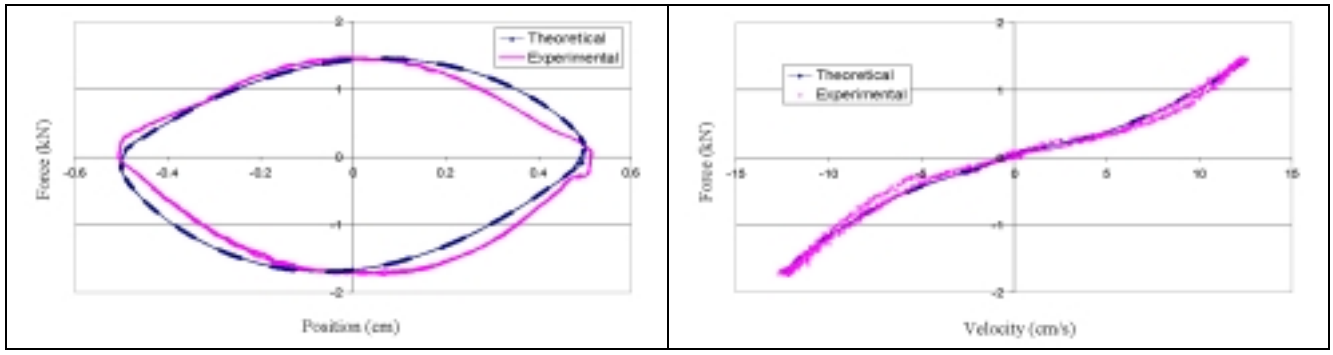

(a) (b)

Figure 26. Theoretical and experimental (a) force-displacement loop and (b) force-velocity relation of the UNR-MRD-005-2 with 4 Hz. and 1 cm. peak to peak amplitude sinusoidal input.

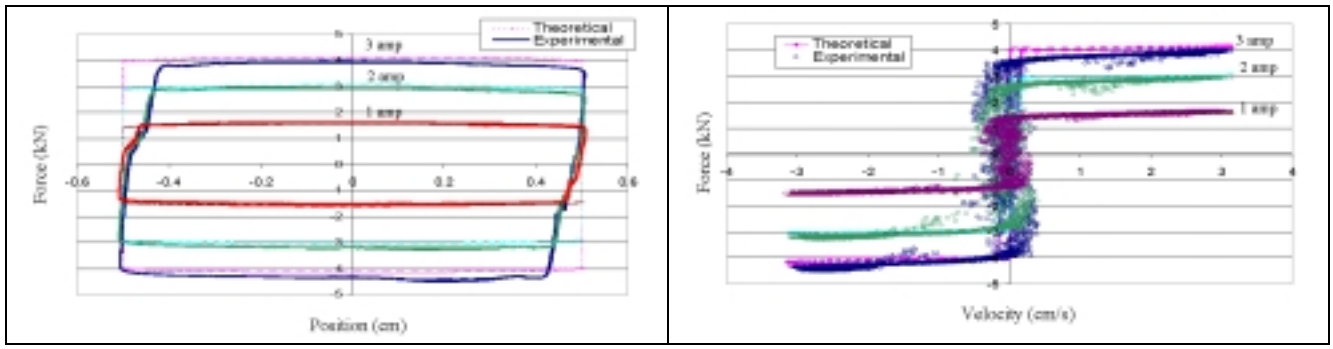

(a) (b)

Figure 27. Theoretical and experimental (a) force-displacement loop and (b) force-velocity relation of the UNR-MRD-005-2 with 1 Hz. and 1 cm. peak to peak amplitude sinusoidal and different electrical current inputs.

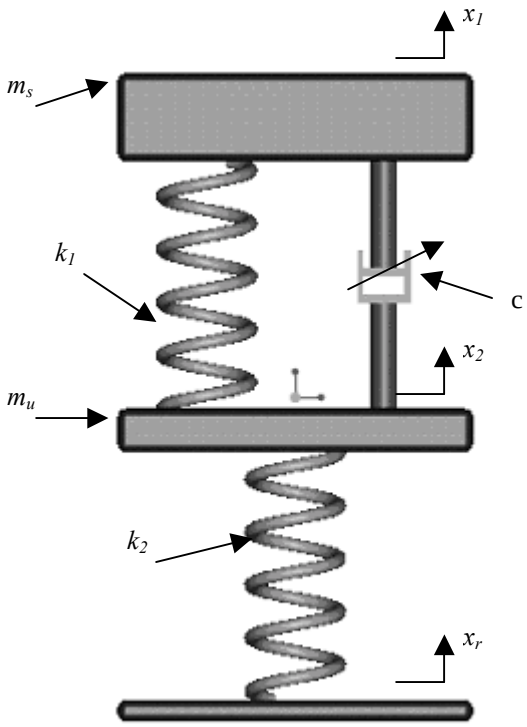

Figure 28. Two degree-of-freedom quarter car model for semi-active HMMWV suspension system.

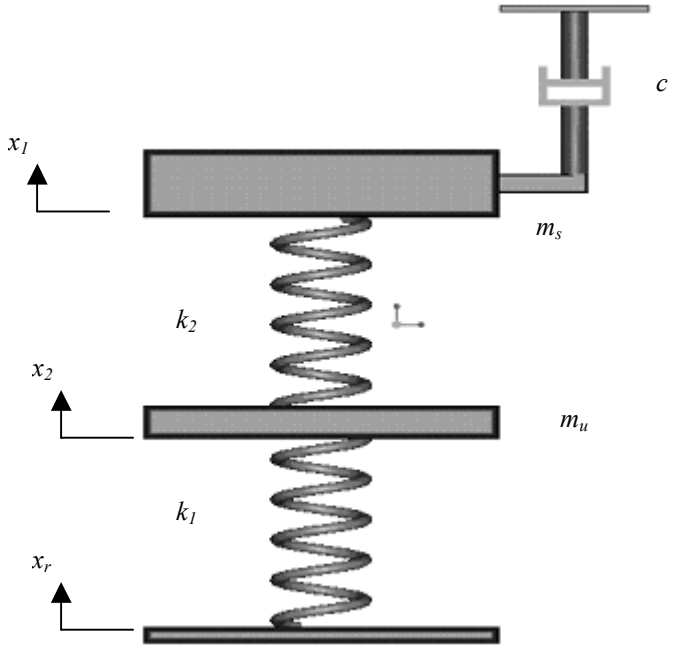

Figure 29. Passive damping representation of the skyhook control in quarter car model.

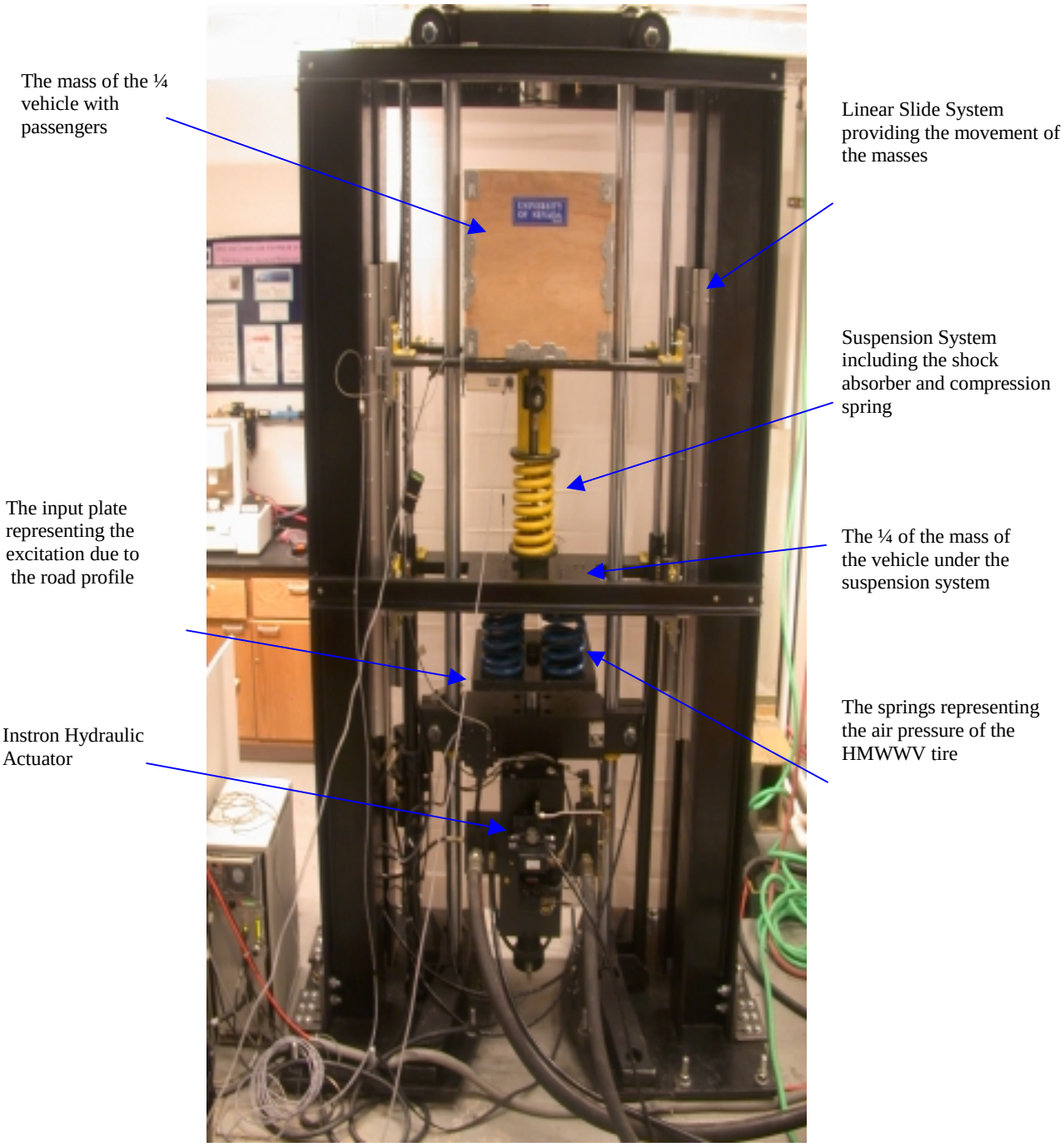

Figure 30. The experimental setup.

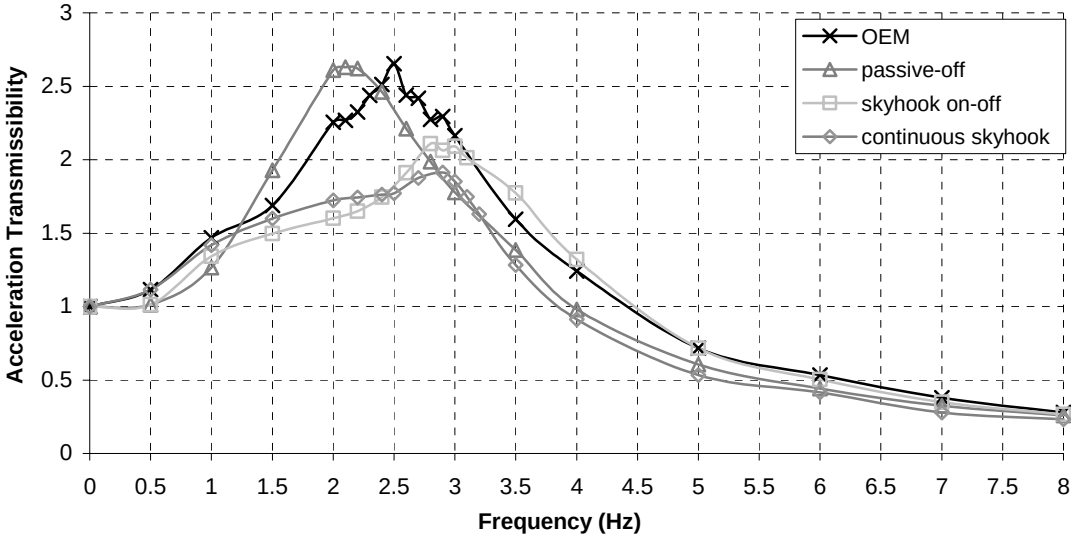

Figure 31. Acceleration transmissibility experimental results of sprung mass for 1cm amplitude input.

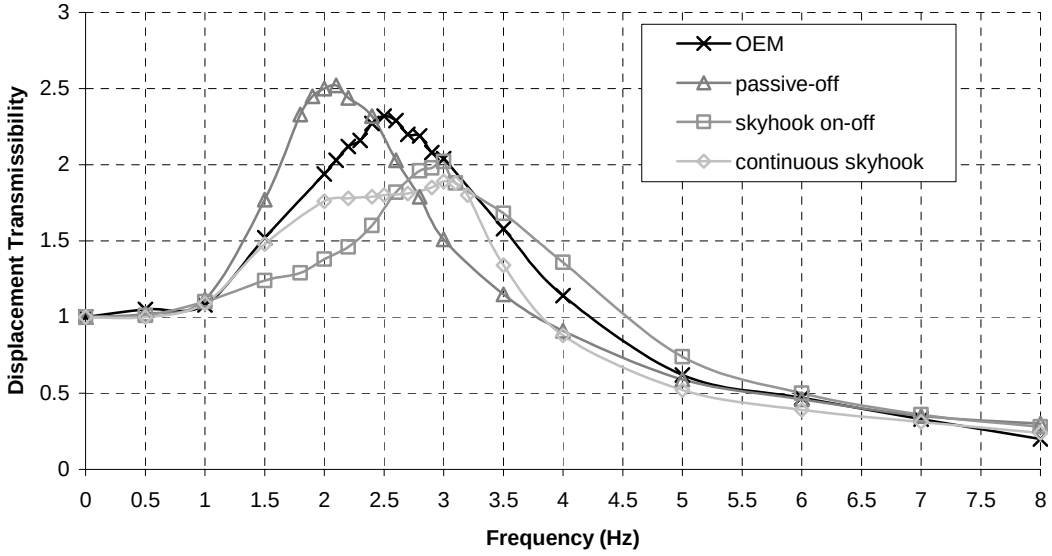

Figure 32. Displacement transmissibility experimental data for the sprung mass with 1 cm amplitude input.

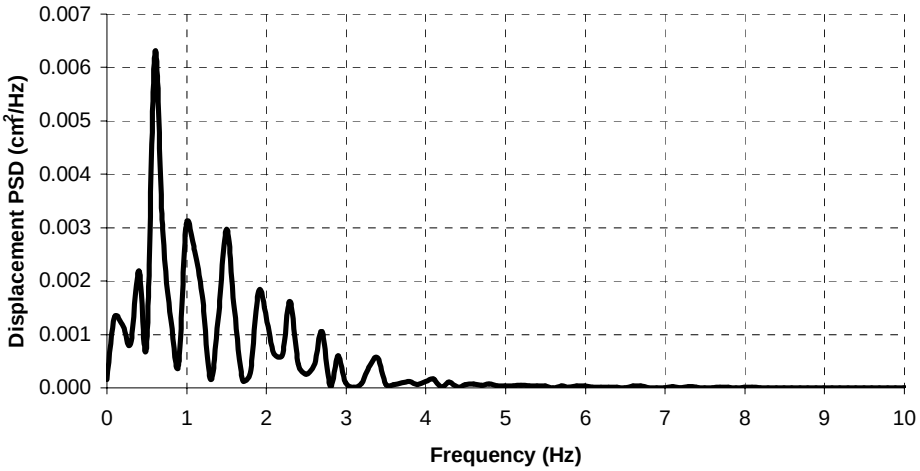

Figure 33. PSD displacement random input.

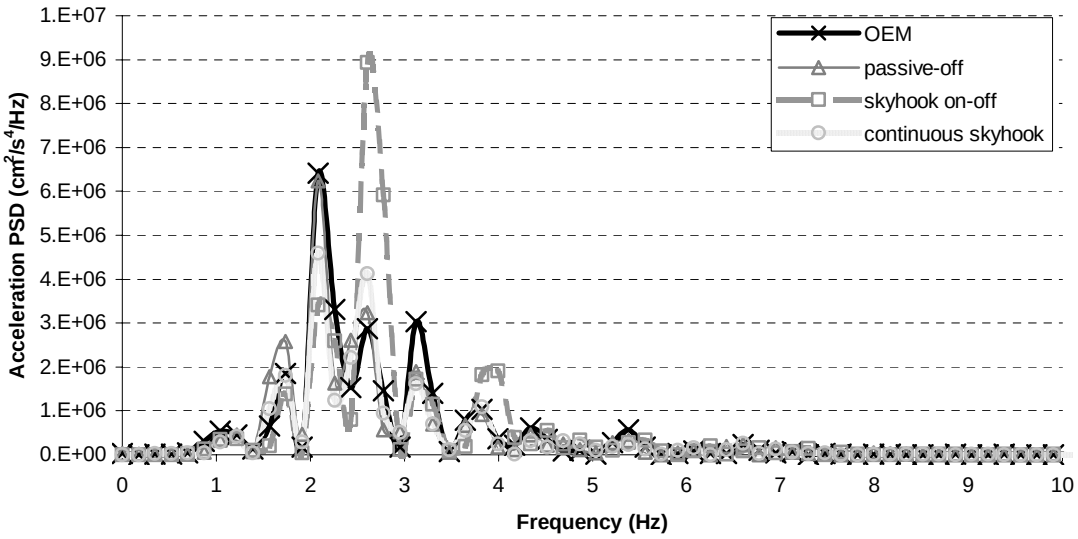

Figure 34. Experimental acceleration PSD of sprung mass under random excitation.

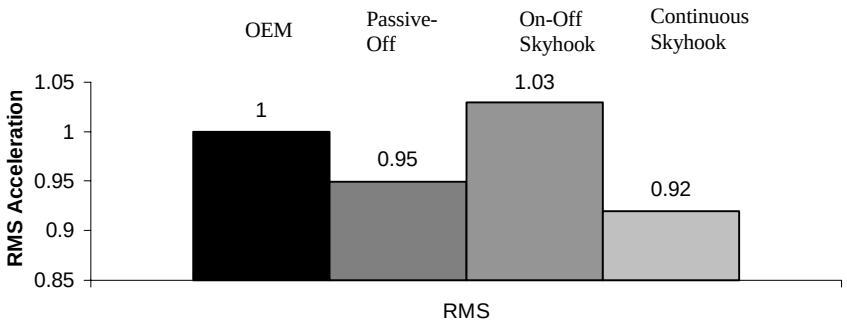

Figure 35. Experimental acceleration RMS of sprung mass under random excitation.

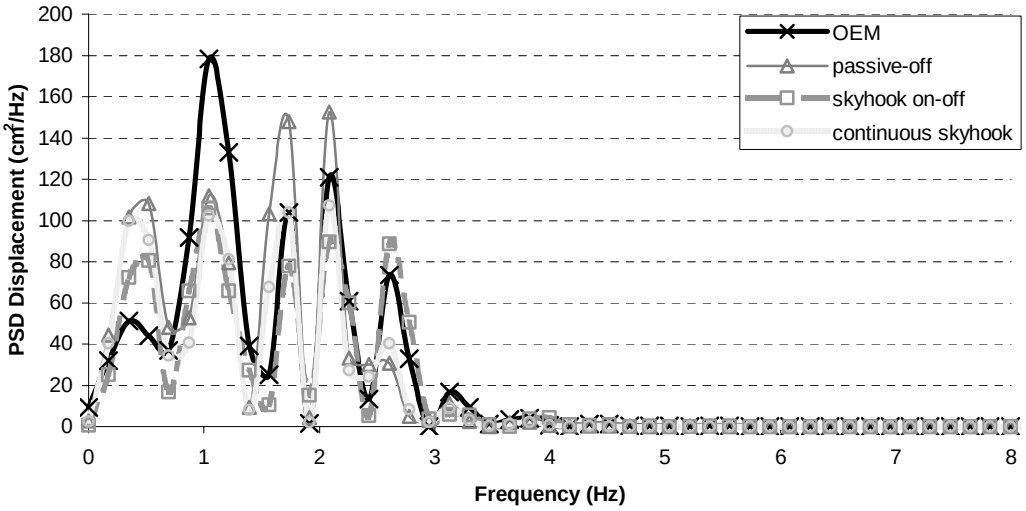

Figure 36. Experimental displacement data of sprung mass under random excitation.

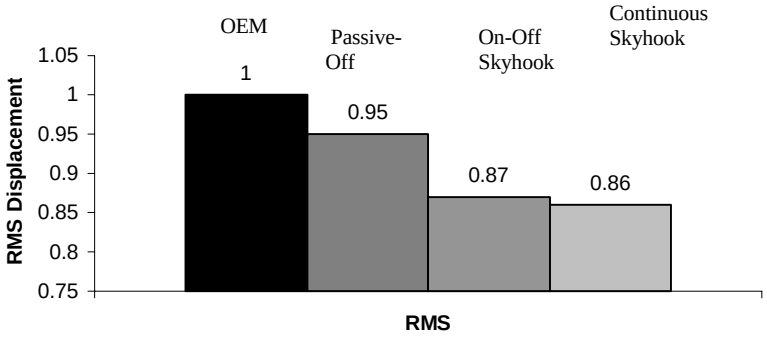

Figure 37. Experimental displacement RMS results.